Propranolol and parathyroid hormone synergistically improve bone volume fraction by suppressing resorption

Annika Treyball, BA[1^], Audrey C. Bergeron, MS[1^], Daniel J. Brooks, MS[2], Kathleen T. Nevola, MS[1,3], Hina Hashmi, BS[1], Kenichi Nagano, DDS, PhD[4], Deborah Barlow[5], Karen L. Houseknecht, PhD[5], Roland Baron, DDS, PhD[4], Mary L. Bouxsein, PhD[2], Anyonya R. Guntur, PhD[1,6], Katherine J. Motyl, PhD[1,6,7]*

[1]Center for Molecular Medicine, Maine Medical Center Research Institute, Scarborough, ME
[2]Center for Advanced Orthopaedic Studies, Beth Israel Deaconess Medical Center, Boston, MA
[3]Tufts Graduate School of Biomedical Sciences, Tufts University, Boston, MA
[4]Department of Oral Medicine, Infection and Immunity, Harvard School of Dental Medicine, Boston, MA
[5]Department of Pharmacology, University of New England, Biddeford, ME
[6]Graduate School of Biomedical Sciences and Engineering, University of Maine, Orono, ME
[7]Tufts University School of Medicine, Tufts University, Boston, MA

^*Annika Treyball and Audrey Bergeron have been assigned co-first authorship.*

Current Affiliations

- Annika Treyball is presently affiliated with the Tufts University School of Medicine.
- Hina Hashmi is presently affiliated with the College of Osteopathic Medicine, University of New England.
- Kenichi Nagano is presently affiliated with the Department of Oral Pathology and Bone Metabolism, Institute of Biomedical Sciences, Nagasaki University.

**Address correspondence to:*
Katherine J. Motyl
81 Research Drive
Scarborough, ME 04074
(207) 396-8004
motylk@mmc.org

Conflict of Interest Statement:
The authors have declared that no conflict of interest exists.

Abstract

Although the non-selective β-blocker, propranolol, improves bone density with PTH treatment in mice, the mechanism of this effect is unclear. To address this, we used a combination of *in vitro* and *in vivo* approaches to address how propranolol influences bone remodeling in the context of PTH treatment. *In vitro*, propranolol amplified the acute, PTH-induced, intracellular calcium signal and elevated *Igf1* expression in osteoblasts. *In vivo,* intermittent PTH and propranolol had synergistic effects in the trabecular bone of the distal femur. The most striking finding was a complete suppression of PTH-induced bone resorption. Despite this, PTH-induced receptor activator of nuclear factor kappa-B ligand (RANKL) mRNA and protein levels were unaltered by propranolol. Interestingly, propranolol suppressed differentiation of primary osteoclasts, suggesting a novel direct influence of propranolol on osteoclasts *in vivo*. Taken together, this work suggests combining propranolol with PTH could be beneficial to patients with extremely low bone density.

57 **Introduction**

58 The sympathetic nervous system (SNS) plays a critical role in the regulation of bone remodeling.
59 The SNS suppresses bone formation and promotes receptor activator of nuclear factor kappa-B
60 ligand (RANKL)-mediated osteoclast recruitment, resulting in low trabecular bone volume
61 fraction in mice (Elefteriou et al., 2005; Takeda et al., 2002). Consistent with this, tyrosine
62 hydroxylase, one of the enzymes involved in norepinephrine production, is present in nerves
63 within bone, marrow, and periosteum (Mach et al., 2002). The major adrenergic receptor
64 mediating downstream effects of norepinephrine appears to be the β2AR in mice (Takeda et al.,
65 2002). Deletion of β2AR, or treatment with the non-selective βAR antagonist (β-blocker)
66 propranolol, prevents bone loss in situations of stress, antipsychotic and antidepressant treatment,
67 and in other situations in which sympathetic signaling to bone may be elevated (Motyl et al.,
68 2015, 2013; Ortuno et al., 2016; Takeda et al., 2002; Yadav et al., 2009; Yirmiya et al., 2006).
69 The majority of studies point toward a mechanism of β2AR suppressing bone formation directly
70 in the osteoblast, and activating bone resorption indirectly, through the RANKL/OPG pathway
71 (Ducy et al., 2000; Elefteriou et al., 2005; Takeda et al., 2002). Indeed, mice with an osteoblast-
72 specific deletion of *Adrb2* have a high bone density phenotype as adults, with increased bone
73 formation and reduced *Rankl* expression (Kajimura et al., 2011). However, some studies have
74 found evidence for direct effects of β2AR signaling in osteoclasts (Kondo et al., 2013; Rodrigues
75 et al., 2012), suggesting the downstream effects of elevated SNS activity may be more complex
76 than generally accepted.

77 Despite this complexity, identifying osteoporosis treatment strategies that modulate
78 sympathetic signaling remains clinically useful. β-blockers are one such class of drugs that has
79 been shown to reduce fracture risk and increase BMD in patients (Yang et al., 2012)(Toulis et

80 al., 2014). Furthermore, rodent studies have shown that combining β-blockers with teriparatide
81 (intermittent truncated parathyroid hormone, PTH) may further promote bone density, but any
82 benefit of combined treatment has not been examined in humans. Evidence from ovariectomized
83 mice suggests that combining PTH treatment with propranolol increases bone mineral density
84 beyond the levels achieved by PTH alone, and histomorphometric analyses indicated that
85 improvement was largely due to increased bone formation and osteoblast number (Pierroz et al.,
86 2006). Recent literature also suggests that PTH-induced bone formation may be at the expense of
87 bone marrow adiposity since osteoblasts and adipocytes arise from a common mesenchymal
88 progenitor (Fan et al., 2017). Furthermore, propranolol has been shown to inhibit marrow
89 adipocyte differentiation, which could, in turn, enhance osteogenesis (Baek et al., 2014). Despite
90 this, how combined PTH and propranolol treatment influences marrow adiposity remains
91 unknown and may be important for understanding the mechanism of improved bone formation
92 with combined treatment.
93 On a cellular level, evidence from *in vitro* and *in vivo* studies suggest that PTH efficacy is
94 dependent upon the presence of the β2AR. Deletion of *Adrb2,* the gene that encodes β2AR,
95 prevents the anabolic effect of intermittent PTH in young and aged mice, suggesting some β2AR
96 signaling is required (Hanyu et al., 2012). One mechanism of this may be through β2AR
97 signaling allowing G-protein βγ (Gβγ) subunit to bind endosomal PTH1R, which sustains cAMP
98 levels leading to enhanced mineralization in osteoblasts (Jean-Alphonse et al., 2017). cAMP
99 signaling, however, is not the only avenue for PTH effects to be transduced to the cell (Gesty-
100 Palmer and Luttrell, 2011)(Cheloha et al., 2015). PTH1R also signals through phospholipase C
101 to increase Ca^{2+} release from intracellular stores, as well as through arrestin-mediated
102 mechanisms (Gesty-Palmer and Luttrell, 2011)(Cheloha et al., 2015). There is an established role

103 for intracellular Ca^{2+} signaling in the regulation of osteoblast differentiation through the
104 calmodulin/CamKII pathway regulating AP-1 and CREB/ATF4 transcription factors (Zayzafoon
105 et al., 2005). It has been shown that silencing of *Adrb2* can increase pCREB (Moriya et al.,
106 2015), but it remains unknown whether combination of PTH treatment with β2AR antagonists
107 would impact these pathways.

108 To further investigate the cellular and systemic effects of co-modulation of PTH1R and
109 β2AR, we performed a series of *in vitro* and *in vivo* assays pharmacologically targeting these
110 receptors. A pharmacological approach was chosen so that any advantages of combination
111 treatments may eventually be translated to humans. Briefly, we determined that the β-blocker
112 propranolol enhanced PTH-induced Ca^{2+} signaling in osteoblast-like cells *in vitro* and that the
113 combination of PTH and propranolol *in vivo* synergistically increased bone volume fraction in
114 the distal femur in part by increasing markers of bone formation. More striking, however, was
115 that propranolol prevented PTH-induced bone resorption, but did not impact PTH-induced
116 changes in RANKL or OPG pathway members. Finally, we identified that this effect may be
117 through direct anti-osteoclastogenic effects of propranolol. In all, these findings suggest that
118 modifications to PTH therapy that mimic outcomes from propranolol treatment, or simply
119 combining PTH with β-blockers, may be a useful approach to minimizing resorption and
120 promoting net bone accrual.
121

122 **Results**

123 *PTH-induced intracellular calcium signaling is enhanced by propranolol*

124 To test the impact of β-blockers on PTH-induced calcium signaling in osteoblasts, we first
125 measured the concentration-dependence of the intracellular Ca^{2+} response to PTH in MC3T3-E1
126 cells differentiated for 7 days (Figure 1A). PTH induced a measurable Ca^{2+} signal at
127 concentrations as low as 10 nM and the peak response was observed at 1 μM. Using a log
128 transformation, we calculated the concentration with 50% of maximal excitation to be 66.64 nM.
129 Therefore, we used a concentration of 100 nM in our studies, to be within the dynamic range of
130 the concentration-response curve, but also within range of previous reports. Next, we found that
131 pre-treatment with propranolol significantly increased the intracellular Ca^{2+} signal induced from
132 PTH (Figure 1B, C).

133 To determine whether combined PTH and propranolol treatment had any functional
134 consequence in osteoblasts, we examined gene expression after acute treatment with PTH,
135 propranolol or both. Although there were no differences in early osteoblastogenic markers *Runx2*
136 and *Sp7* (not shown), PTH induced *Osteocalcin* expression (main effect of PTH p=0.016)
137 similarly in both vehicle and propranolol treated cells, although only the group treated with PTH
138 alone (no propranolol present) reached pairwise statistical significance (Figure 1D, E). Because
139 intracellular Ca^{2+} has been shown to modulate AP-1 family transcription factors, we examined
140 gene expression of *Fos.* Interestingly, the PTH-induced increase in *Fos* was higher when
141 propranolol was present (Figure 1F), consistent propranolol promoting PTH-induced intracellular
142 Ca^{2+} levels. One established mechanism of osteoanabolism from PTH is through increased
143 expression and autocrine signaling of IGF-1 (Esen et al., 2015). We found a significant increase
144 in *Igf1* expression only in the PTH and propranolol co-treated group (Figure 1G). These findings

Figure 1

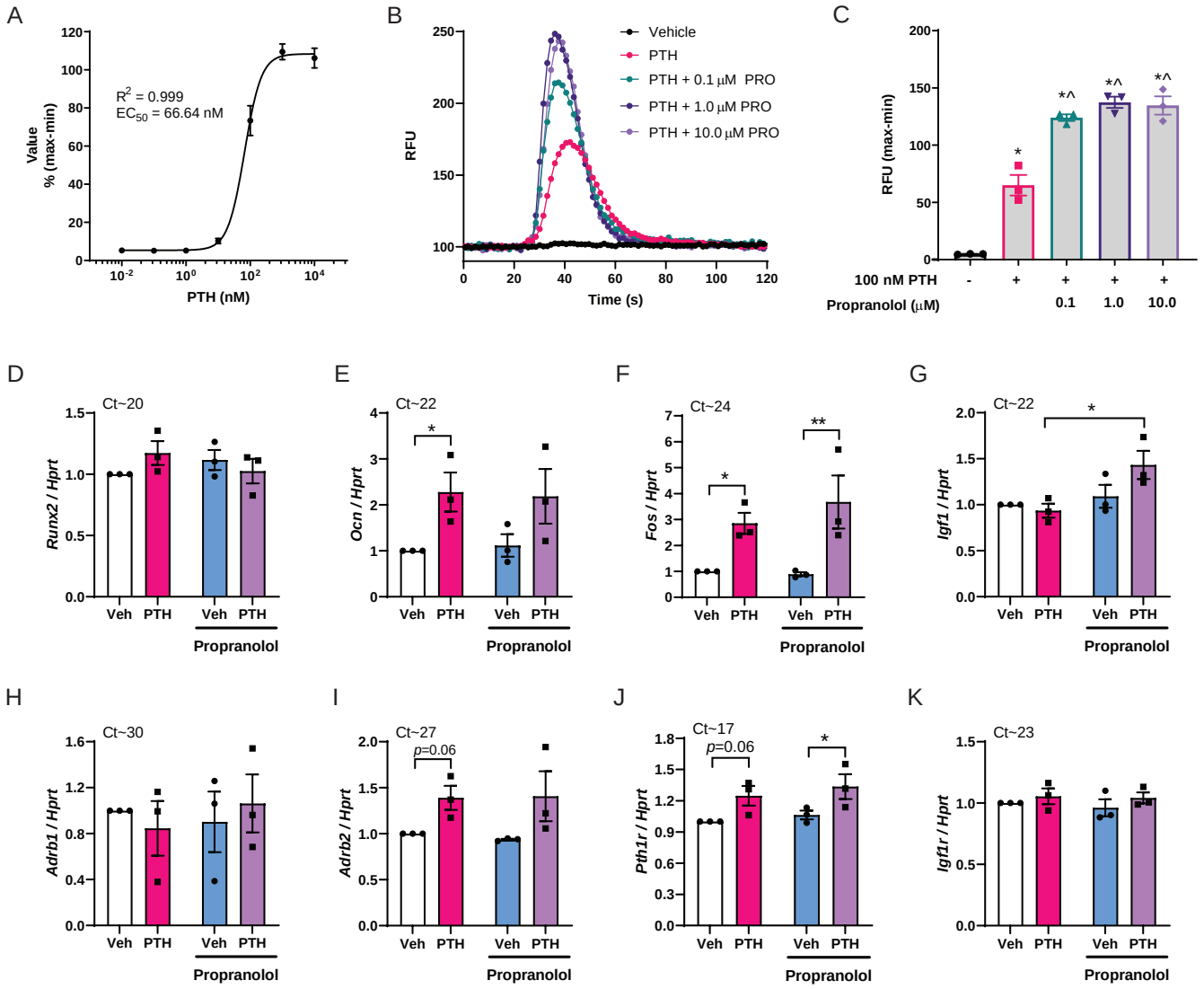

Figure 1. β-blocker propranolol potentiated osteoblast intracellular Ca^{2+} and *Igf1* expression. MC3T3-E1 cells were differentiated to day 7 in osteogenic media. (A) Fluorescence ratio indicative of intracellular Ca^{2+} concentrations was expressed as a percentage of the maximum level. (B) Representative traces of 100 nM PTH-induced fluorescence over time with pretreatment of vehicle, or 0.1, 1 or 10 μM propranolol. (C) Quantification of the maximum-minimum PTH-induced Ca^{2+} fluorescence after pretreatment with vehicle or propranolol. One representative of three experiments (each performed in triplicate) is shown. *p<0.05 compared to vehicle-treated (black), ^p<0.05 compared to 100 nM PTH-treated (pink) by Tukey's post-hoc test after significant one-way ANOVA. (D-K) Gene expression of *Runx2*, *Ocn*, *Fos*, *Igf1*, *Adrb1*, *Adrb2*, *Pth1r* and *Igf1r* in MC3T3-E1 cells at day 7 after 1 hour treatment with vehicle (white), 100 nM PTH (pink), 1 μM propranolol (blue) or 100 nM PTH + 1 μM propranolol (purple). Genes are normalized to non-modulated housekeeping gene, *Hprt*. Each data point represents the mean from an independent experiment, performed in triplicate. Expression levels in vehicle-treated cells from each experiment were set to 1. Approximate Ct values of vehicle-treated groups are shown above each graph. Bars represent mean of the three independent experiments ± SEM. *p<0.05, **p<0.01 by Holm-Sidak post hoc test after a significant two-way ANOVA.

145 suggest propranolol may improve bone formation from PTH through increasing intracellular
146 Ca^{2+} signaling and promoting expression of *Igf1*.
147 To ensure the relevant receptors were present in MC3T3-E1 cells at day 7 of
148 differentiation, we also examined *Adrb1, Adrb2, Pth1r* and *Igf1r* (Figure 1, H-K). *Adrb1*
149 expression was low and variable, but *Adrb2* was more highly expressed and there was a trend
150 toward increased expression with PTH treatment. Furthermore, both *Pth1r* and *Igf1r* were highly
151 expressed and the expression levels of *Pth1r* also increased with PTH treatment, reaching
152 statistical significance in the propranolol treated group. Thus, co-treatment with propranolol
153 appears to promote PTH-induced Ca^{2+} flux, as well as *Igf1* and *Pth1r* expression. It is well-
154 established that long-term PTH treatment *in vitro* does not model the *in vivo* anabolic effects of
155 intermittent PTH therapy. Therefore, to test whether these acute effects had long-term
156 consequences we moved to *in vivo* studies.
157
158 *Propranolol improved total BMD in the presence of PTH*
159 To test whether propranolol would improve PTH-induced bone formation, we treated mice with
160 either vehicle, PTH, propranolol, or PTH + propranolol from 16-20 weeks of age. Neither body
161 weight, fat mass, nor fat-free mass was altered in any of the treatment groups, suggesting that
162 any bone changes would be independent of differences in loading (Table I). As expected, PTH
163 had a significant main effect on total and femoral aBMD and aBMC (Table I). Although
164 propranolol only had a significant main effect on total aBMD, all bone parameters measured by
165 DXA were highest in the PTH + propranolol group (Table I). Interestingly, co-treatment with
166 PTH and propranolol increased total aBMD beyond that caused by PTH or propranolol alone.
167

Table I. Body composition and areal bone parameters from mice treated with PTH and/or propranolol.

	Vehicle (N=10)	PTH (N=11)	Propranolol (N=9)	PTH + Propranolol (N=11)	2-way ANOVA *p*-values		
					PTH	Propranolol	Interaction
Body Mass (g)	21.8 ± 0.5	22.5 ± 0.4	21.7 ± 0.3	22.6 ± 0.4	*ns*	*ns*	*ns*
Lean Mass (g)	17.4 ± 0.4	17.9 ± 0.3	18.0 ± 0.3	17.9 ± 0.3	*ns*	*ns*	*ns*
Fat Mass (g)	2.6 ± 0.1	2.5 ± 0.2	2.6 ± 0.2	2.7 ± 0.2	*ns*	*ns*	*ns*
Total aBMD (g/cm^2)	0.0527 ± 0.0003	0.0544 ± 0.0004**	0.0535 ± 0.0004	0.0559 ± 0.0003^##	<0.01	<0.01	*ns*
Femur aBMD (g/cm^2)	0.0620 ± 0.0006	0.0655 ± 0.0008	0.0628 ± 0.0016	0.0678 ± 0.0008##	<0.01	*ns*	*ns*
Total aBMC (g)	0.438 ± 0.006	0.463 ± 0.006	0.444 ± 0.007	0.475 ± 0.009#	<0.01	*ns*	*ns*
Femur aBMC (g)	0.0097 ± 0.0002	0.0102 ± 0.0003	0.0093 ± 0.0003	0.0105 ± 0.0002##	<0.01	*ns*	*ns*

*$p<0.05$, **$p<0.01$ compared to vehicle group.

^$p<0.05$, ^^$p<0.01$ compared to PTH group.

#$p<0.05$, ##$p<0.01$ compared to propranolol group.

168 *PTH and propranolol had site-specific effects on trabecular bone microarchitecture*

169 To investigate the impact of PTH and propranolol treatment on bone microarchitecture, we
170 performed μCT on L5 vertebrae and femurs. Propranolol and PTH both independently improved
171 trabecular BV/TV of the L5 vertebra, but the combination of PTH and propranolol improved
172 BV/TV and BMD above and beyond that of either treatment alone (Figure 2). This is likely due
173 to a combined effect of increased trabecular thickness and increased trabecular number, the latter
174 of which was only significantly increased by PTH when propranolol was present. Consistent
175 with this, PTH and propranolol together significantly reduced BS/BV ratio compared to
176 propranolol alone (Figure 2).

177 In the distal femur, we focused our examination of PTH and propranolol effects on two
178 distinct sites, the primary and secondary spongiosa (Figure 3). In the secondary spongiosa, PTH
179 increased Tb. BV/TV, BMD, and Conn.D and these parameters were all increased further by
180 combined treatment with propranolol (Figure 3B-D). Although some parameters (Tb.N, Tb.Th,
181 Tb.Sp, and BS/BV) were not altered by PTH alone, the combination reduced SMI, Tb.Sp, and
182 BS/BV, while significantly increasing Tb.N and Tb.Th (Figure 3E-I). The primary spongiosa
183 also had striking changes from PTH, including increased BV/TV, BV and BMD (Figure 3J-L),
184 but these were not exacerbated or diminished by combination PTH and propranolol treatment.
185 Tissue mineral density (TMD), a measurement of the density of the bone itself (not including any
186 marrow), was suppressed with PTH treatment, suggesting that mineral deposition may be
187 compromised (Figure 3M). Interestingly, however, propranolol significantly elevated TMD in
188 PTH-treated mice such that is was not different from vehicle-treated (Figure 3M). This indicates
189 the quality of mineralization in the primary spongiosa during combination PTH and propranolol
190 treatment may be improved compared to PTH alone.

Figure 2

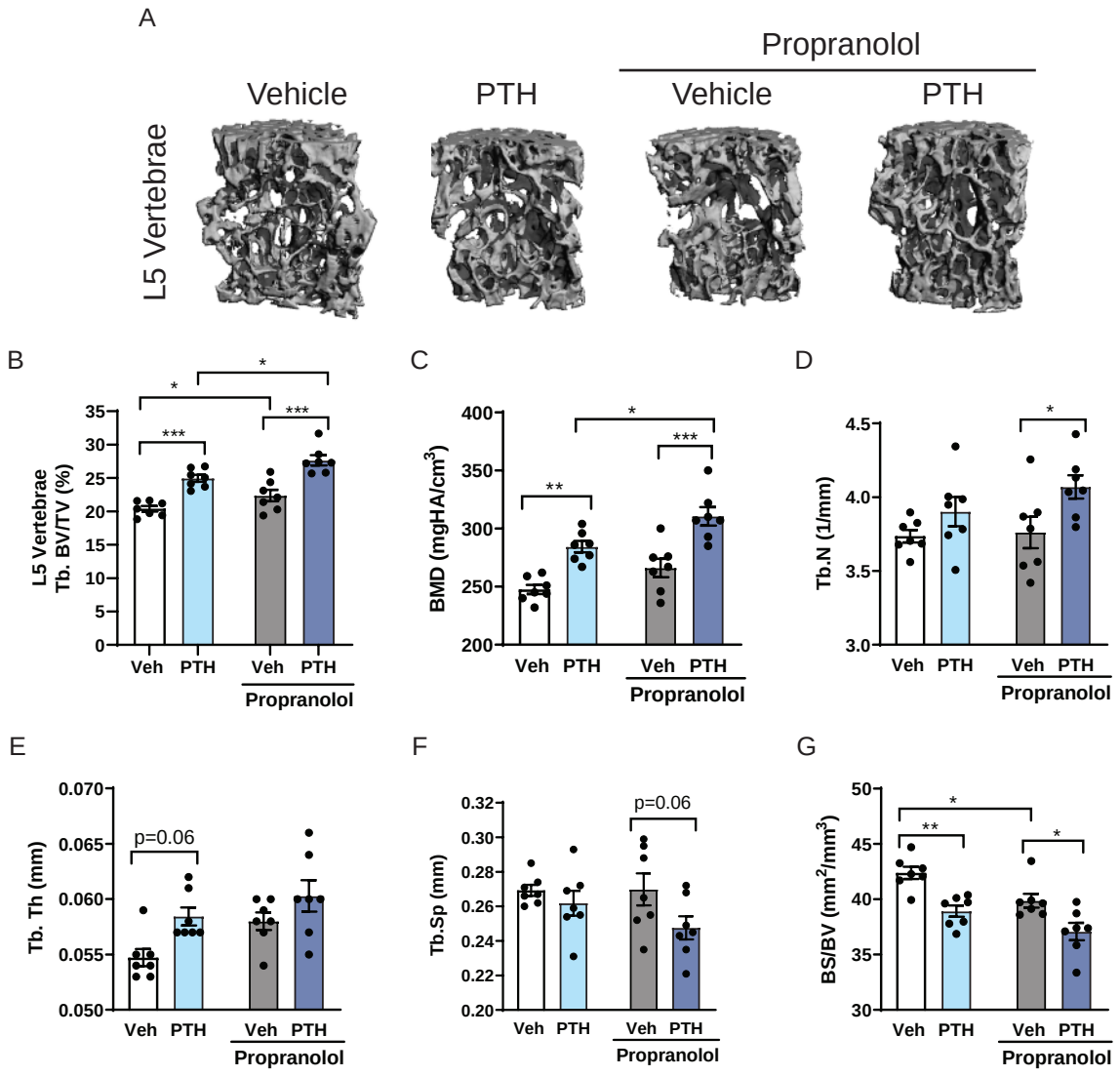

Figure 2. Propranolol improved the positive effects of PTH on trabecular bone in the L5 vertebrae. Mice were treated with vehicle (white), 80 µg/kg PTH (light blue), 0.5 mg/ml propranolol (gray), or PTH and propranolol (dark blue) for 4 weeks, from 16-20 weeks of age. (A) Representative µCT images from L5 vertebrae. (B-G) Trabecular bone volume fraction (Tb. BV/TV), bone mineral density (BMD), number (Tb.N), thickness (Tb.Th), separation (Tb.Sp), and bone surface/bone volume (BS/BV). Bars represent mean +/- standard error. *p<0.05, **p<0.01 by Holm-Sidak post hoc test after a significant two-way ANOVA.

Figure 3

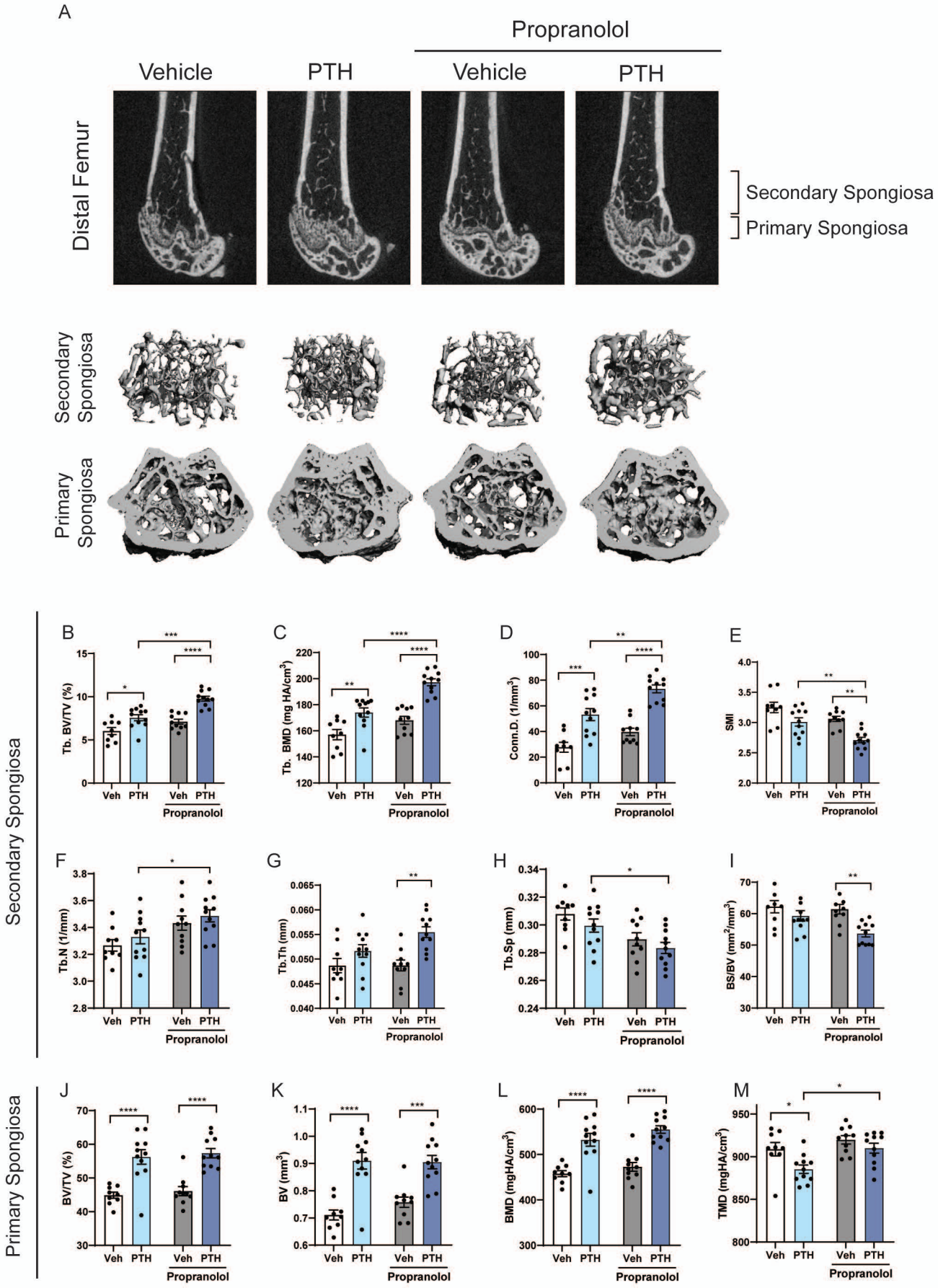
A
Propranolol
Vehicle
PTH
Vehicle
PTH
Distal Femur
Secondary Spongiosa
Primary Spongiosa
Secondary Spongiosa
Primary Spongiosa
Secondary Spongiosa
Primary Spongiosa
B
Tb. BV/TV (%)
C
Tb. BMD (mg HA/cm³)
D
Conn.D. (1/mm³)
E
SMI
F
Tb.N (1/mm)
G
Tb.Th (mm)
H
Tb.Sp (mm)
I
BS/BV (mm²/mm³)
J
BV/TV (%)
K
BV (mm³)
L
BMD (mgHA/cm³)
M
TMD (mgHA/cm³)
Veh
PTH
Veh
PTH
Propranolol

Figure 3. Trabecular bone in the femur secondary spongiosa is enhanced by combination PTH and propranolol treatment. Mice were treated with vehicle (white), 80 µg/kg PTH (light blue), 0.5 mg/ml propranolol (gray), or PTH and propranolol (dark blue) for 4 weeks, from 16-20 weeks of age. (A) Representative 2D (top) and 3D (bottom) images of trabecular micro architecture in the primary and secondary spongiosa of the distal femur. (B-I) Trabecular microarchitectural parameters from the secondary spongiosa. (J-K) Volumetric and densitometric measurements from the primary spongiosa. Bars represent mean +/- standard error. *$p<0.05$, **$p<0.01$, ***$p<0.001$, ****$p<0.0001$ by Holm-Sidak post hoc test after a significant two-way ANOVA.

191

192 *Cortical bone microarchitecture*

193 PTH significantly increased cortical area (Ct.Ar) and polar moment of inertia (pMOI) in the
194 femur midshaft, but did not significantly impact marrow area (Ma.Ar), total area (Tt.Ar), cortical
195 thickness (Ct.Th), tissue mineral density (TMD) or porosity (Figure 4 A-H). Although
196 propranolol treatment did not impact these parameters on its own, propranolol significantly
197 improved the effect of PTH on the cortical bone such that Ct.Ar, Ct.Ar/Tt.Ar, Ct.Th and TMD
198 were elevated in the PTH + propranolol group compared to propranolol alone (Figure 4A, D, E,
199 and F). The increased Ct.Ar/Tt.Ar with combination treatment is most likely due to a reduction
200 in Ma.Ar, because Tt.Ar was clearly unchanged (Figure 4B-D).

201

202 *Propranolol promoted bone formation in PTH-treated mice.*

203 To determine whether co-treatment with propranolol modulated the effect of PTH on bone
204 formation, we performed serum, histomorphometric, and mRNA analyses to evaluate bone
205 remodeling activity. As expected, PTH increased the serum marker of bone formation, P1NP,
206 and this was further increased by co-treatment with PTH and propranolol (Figure 5A).
207 Histomorphometric analyses in the L5 vertebrae indicated a significant effect of PTH by 2-way
208 ANOVA on MAR and BFR parameters (Figure 5B, C). Similarly, osteoblast parameters were
209 elevated by PTH, but were not significantly modulated by the combination with propranolol.
210 However, propranolol did not have a significant main effect on these parameters (except to
211 decrease the N.Ob/B.Pm) and, when combined with PTH, did not increase these indices beyond
212 the level of PTH alone (Figure 5B, C). Propranolol did, however, reduce the amount of OS/BS in
213 PTH-treated mice (Figure 5C).

Figure 4

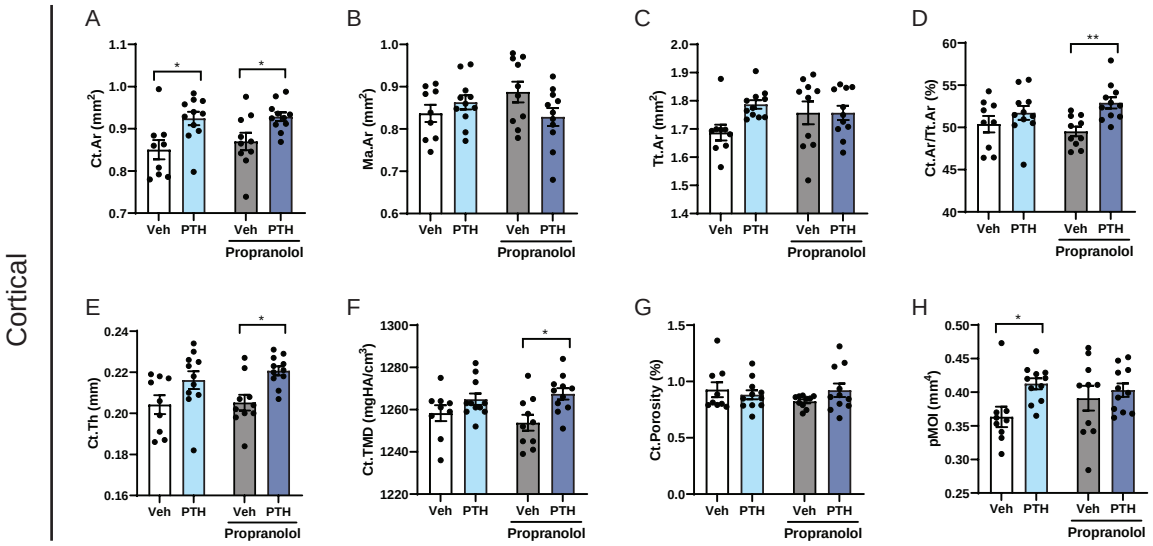

Figure 4. Propranolol improved cortical thickness and density in PTH-treated mice. Mice were treated with vehicle (white), 80 µg/kg PTH (light blue), 0.5 mg/ml propranolol (gray), or PTH and propranolol (dark blue) for 4 weeks, from 16-20 weeks of age. (A-H) Cortical bone microarchitectural parameters, cortical area (Ct.Ar), marrow area (Ma.Ar), total area (Tt.Ar) cortical area fraction (Ct.Ar/Tt.Ar), cortical thickness (Ct.Th), cortical tissue mineral density (Ct.TMD), cortical porosity, and polar moment of inertia (pMOI) were analyzed at the midshaft of the femur. Bars represent mean +/- standard error. *p<0.05, **p<0.01 by Holm-Sidak post hoc test after a significant two-way ANOVA.

Figure 5

A

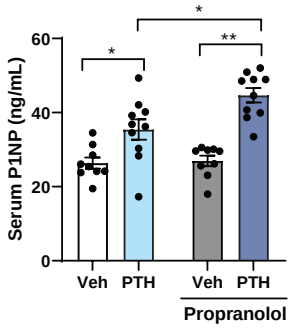

B

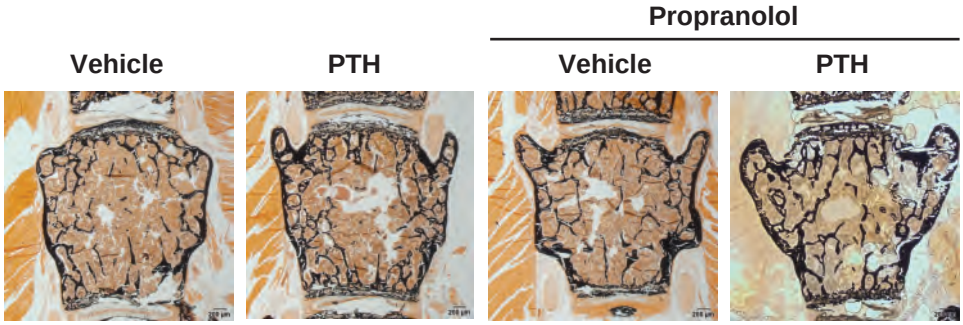

C

	Vehicle (N=7)	PTH (N=7)	Propranolol (N=7)	PTH + Propranolol (N=9)	2-way ANOVA *p*-values PTH	Propranolol	Interaction
BV/TV (%)	9.4 ± 0.8	14.0 ± 0.9**	10.3 ± 0.9	15.6 ± 0.4##	<0.01	*ns*	*ns*
Tb.Th (µm)	37.5 ± 1.7	43.5 ± 2.1*	39.0 ± 1.6	45.0 ± 1.5#	<0.01	*ns*	*ns*
Tb.N (mm^{-1})	2.5 ± 0.1	3.2 ± 0.1**	2.6 ± 0.2	3.5 ± 0.1##	<0.01	*ns*	*ns*
Tb.Sp (µm)	376 ± 20	273 ± 14**	349 ± 24	246 ± 8##	<0.01	*ns*	*ns*
MAR (µm/day)†	1.19 ± 0.07	1.65 ± 0.07**	1.12 ± 0.13	1.65 ± 0.07##	<0.01	*ns*	*ns*
MS/BS (%)†	38.3 ± 2.1	42.3 ± 2.2	39.8 ± 3.3	37.3 ± 4.1	*ns*	*ns*	*ns*
BFR/BV (%/day)†	2.58 ± 0.21	3.61 ± 0.36	2.21 ± 0.26	3.08 ± 0.50	0.01	*ns*	*ns*
BFR/TV (%/day)†	0.23 ± 0.02	0.45 ± 0.05*	0.25 ± 0.05	0.46 ± 0.09#	<0.01	*ns*	*ns*
BFR/BS ($\mu m^3/\mu m^2$/day)†	0.45 ± 0.04	0.70 ± 0.06*	0.45 ± 0.06	0.62 ± 0.08	<0.01	*ns*	*ns*
N.Ob/B.Pm (mm^{-1})	14.7 ± 1.0	22.5 ± 1.5**	12.4 ± 0.6	19.4 ± 1.2##	<0.01	0.03	*ns*
N.Ob/T.Ar (mm^{-2})	71.1 ± 8.5	147.7 ± 6.5**	64.4 ± 3.7	127.0 ± 7.9##	<0.01	*ns*	*ns*
Ob.S/B.Pm (%)	17.4 ± 1.2	26.8 ± 1.8**	14.8 ± 0.8	24.2 ± 1.4##	<0.01	*ns*	*ns*
OS/BS (%)	14.1 ± 1.2	18.8 ± 2.0	13.3 ± 1.3	12.5 ± 1.2^^	*ns*	0.02	*ns*
O.Th (µm)	2.69 ± 0.13	3.14 ± 0.14	2.71 ± 0.27	2.76 ± 0.12	*ns*	*ns*	*ns*

*p<0.05 compared to vehicle, **p<0.01 compared to vehicle
^p<0.05 compared to PTH, ^^p<0.01 compared to PTH
#p<0.05 compared to PRO, ##p<0.01 compared to PRO
†N=4-5 for dynamic measurements.

D

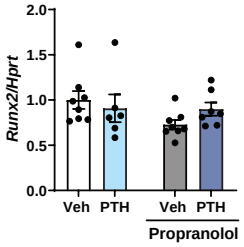

E

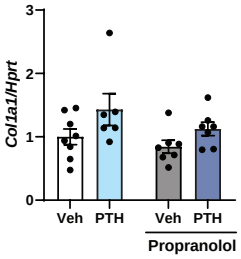

F

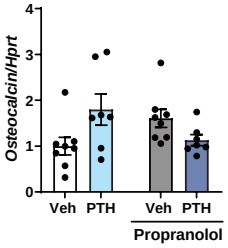

G

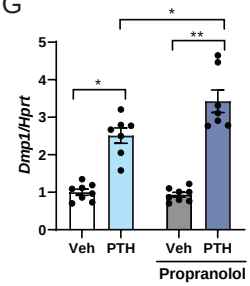

H

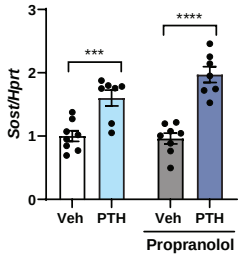

Figure 5. Propranolol improved bone formation markers in PTH-treated mice. Mice were treated with vehicle (white), 80 µg/kg PTH (light blue), 0.5 mg/ml propranolol (gray), or PTH and propranolol (dark blue) for 4 weeks, from 16-20 weeks of age. (A) Serum P1NP was measured by ELISA. (B-C) Static and dynamic histomorphometry representative images and quantification of architectural, bone formation and osteoblast parameters measured in L5 vertebrae. (D-H) Gene expression of markers of bone formation and osteoblast maturity were analyzed in the tibia and normalized by the non-modulated housekeeping gene, *Hprt*. Bars represent mean +/- standard error. *p<0.05, **p<0.01 by Holm-Sidak post hoc test after a significant two-way ANOVA.

214 In general, these findings contrast the serum P1NP finding. Therefore, we examined
215 mRNA markers of osteoblastogenesis and osteocyte maturation in the tibia. Although we did not
216 see significant differences in *Runx2*, *Col1a1*, or *Osteocalcin* expression (Figure 5D-F), we did
217 observe differences in late osteoblast and osteocyte markers. First, dentin matrix acidic
218 phosphoprotein 1 (*Dmp1*) expression was increased with PTH treatment, but there was also a
219 significant interaction (p=0.01) such that PTH-induced *Dmp1* expression was higher in the
220 propranolol treated group, while propranolol alone had no effect in the absence of PTH (Figure
221 5G). Surprisingly, intermittent treatment with PTH induced *Sost* expression, in contrast to
222 previously reported effects with chronic elevation, and *Sost* was elevated to a greater degree in
223 propranolol treated mice (Figure 5H) (Bellido et al., 2005). Although serum P1NP is elevated,
224 changes in bone formation (histological and mRNA-based) do not convincingly explain the
225 improved BV/TV in mice treated with PTH and propranolol.
226
227 *Bone marrow adipocytes*
228 Recent studies have suggested PTH may suppress bone marrow adipose tissue (BMAT) as a
229 means or consequence of promoting bone formation. Although marrow adipocyte size was not
230 influenced by PTH, there was a significant interaction effect ($p<0.05$) of PTH and propranolol in
231 both adipocyte volume / total volume (AV/TV) and adipocyte number parameters. In particular,
232 PTH tended to reduce marrow adipocyte numbers in mice not treated with propranolol (p=0.08)
233 but this effect was blunted in propranolol-treated mice (Figure S1).
234
235 *PTH-induced osteoclast differentiation and activity was blocked by propranolol*

Figure S1

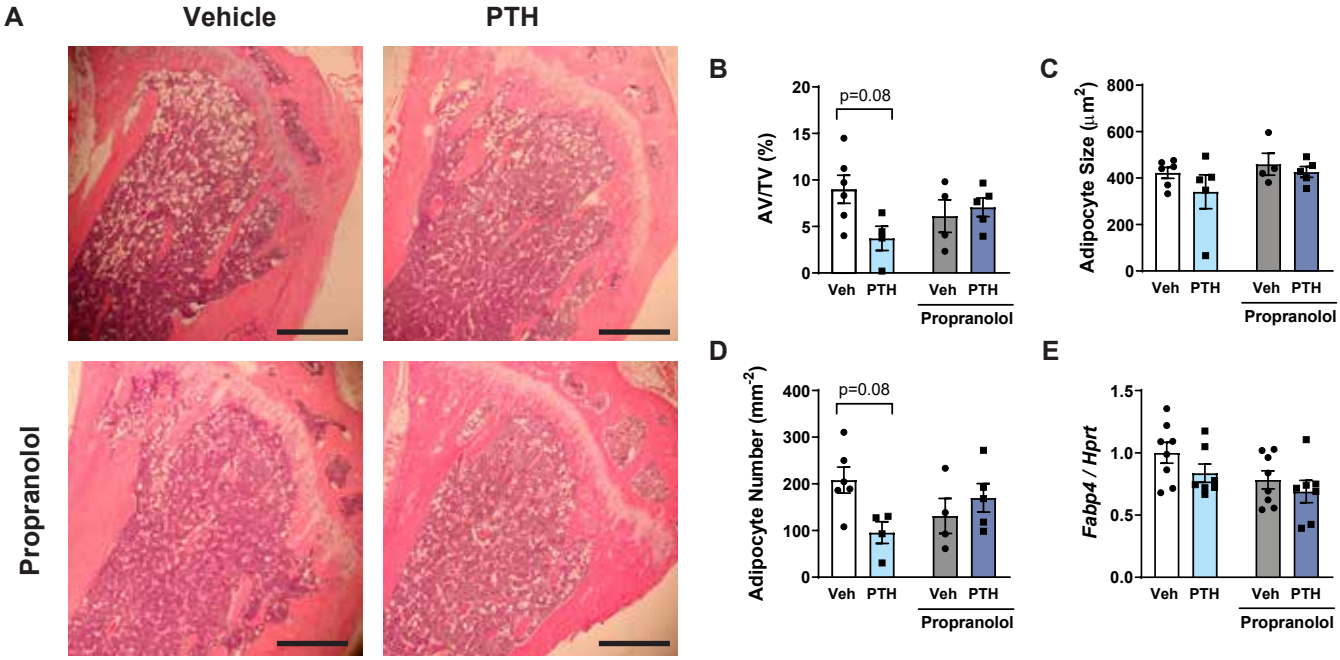
A
Vehicle
PTH
Propranolol
B
AV/TV (%)
p=0.08
Veh
PTH
Propranolol
C
Adipocyte Size (μm²)
D
Adipocyte Number (mm⁻²)
E
Fabp4 / Hprt

236 Consistent with the known effect of PTH to increase resorption, PTH increased expression of
237 *Ctsk* and *Trap5*, as well as the serum protein levels of the resorption marker CTx (Figure 6A-C).
238 Interestingly, propranolol prevented the PTH-induced increase in *Trap5* expression and serum
239 CTx, suggesting propranolol prevents PTH-induced resorption (Figure 6B, C). Consistent with
240 the literature, histomorphometry indicated that PTH increased the number of osteoclasts
241 (N.Oc/T.Ar, Figure 6D). Propranolol alone did not have any impact on the number of osteoclasts
242 or the other osteoclast parameters (Figure 6D). When combined, however, the number of
243 osteoclasts (N.Oc/B.Pm and N.Oc/T.Ar) and the osteoclast surface fraction (Oc.S/BS) was lower
244 in mice treated with PTH and propranolol compared to those treated with PTH alone (Figure
245 6D), interaction $p \leq 0.02$). Notably, the PTH-induced increase in N.Oc/T.Ar was completely
246 blocked by co-treatment with propranolol ($p<0.01$, Figure 6D). All three lines of evidence related
247 to osteoclasts (serum, mRNA, and histomorphometry) point toward a strong effect of propranolol
248 to reduce PTH-induced bone resorption.
249 Propranolol can centrally suppress sympathetic activity, therefore we measured
250 norepinephrine (NE) levels in serum as well. While neither PTH nor propranolol independently
251 modulated NE, the combination treatment resulted in significantly lower circulating NE
252 compared to PTH alone (Figure 6E), suggesting a systemic lowering of sympathetic signaling by
253 propranolol might be responsible for the suppressed resorption. Because the current
254 understanding of the mechanism of NE signaling-induced osteoclastogenesis is through the
255 modulation of *receptor activator of nuclear factor kappa-B ligand* (*Rankl*) expression in the
256 osteoblast, we measured circulating RANKL and found that, to our surprise, propranolol had no
257 effect on PTH-induced RANKL levels (Figure 6F). Furthermore, although PTH induced *Rankl*
258 gene expression in cortical bone as expected, propranolol did not have any blunting effect on

Figure 6

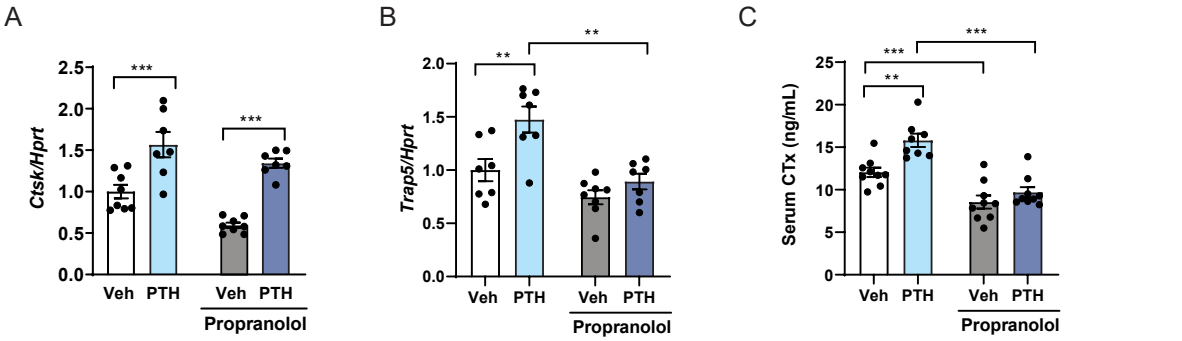

D

	Vehicle (N=7)	PTH (N=7)	Propranolol (N=7)	PTH + Propranolol (N=9)	2-way ANOVA *p*-values		
					PTH	Propranolol	Interaction
N.Oc/B.Pm (mm^{-1})	5.9 ± 0.3	6.2 ± 0.2	5.3 ± 0.4	4.2 ± 0.2$^{\#}$,^^	*ns*	<0.01	0.02
N.Oc/T.Ar (mm^{-2})	28.2 ± 2.4	41.3 ± 2.4**	27.4 ± 1.9	27.7 ± 1.5^^	<0.01	<0.01	<0.01
Oc.S/B.Pm (%)	14.8 ± 0.8	15.9 ± 0.5	13.1 ± 0.9	10.6 ± 0.5^^	*ns*	<0.01	0.02
ES/BS (%)	5.9 ± 0.5	5.8 ± 0.4	5.0 ± 0.7	4.1 ± 0.3^	*ns*	0.01	*ns*
*p<0.05 compared to vehicle, **p<0.01 compared to vehicle							
^p<0.05 compared to PTH, ^^p<0.01 compared to PTH							
$^{\#}p$<0.05 compared to PRO, ##p<0.01 compared to PRO							

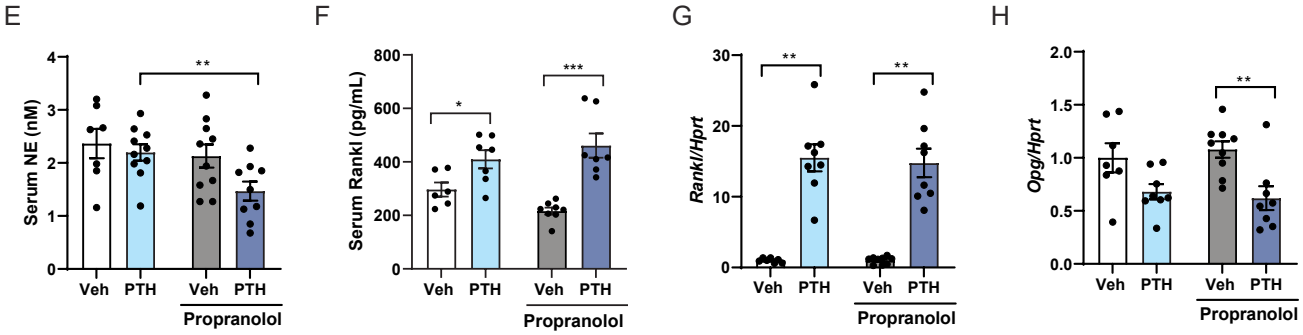

259 *Rankl* (Figure 6G), but did lower *Opg* (Figure 6H), suggesting other mechanisms were
260 responsible for the reduced osteoclast numbers and CTx levels in PTH and propranolol treated
261 mice.
262
263 *Propranolol directly inhibits osteoclast differentiation and function*
264 Because propranolol blocked resorption *in vivo* without modulating the RANKL/OPG pathway
265 members we examined, we hypothesized that osteoclasts may respond directly to propranolol.
266 We first accessed publicly available microarray data from RAW264.7 cells treated for 48 hours
267 with RANKL and vehicle. The detection levels of *Adrb1* and *Adrb3* were only slightly higher or
268 equivalent to those of *Bglap* and *Mcsf,* which are not expressed in osteoclasts, suggesting *Adrb1*
269 and *Adrb3* had little to no detectable expression (Figure 7A). *Adrb2* was detected at a higher
270 level, comparable to the amount of *Ctsk* before RANKL addition. However, *Adrb2* levels were
271 not as high as other classically expressed osteoclast genes (*Cfms*, *Nfat1*), and were not changed
272 with RANKL addition (Figure 7A). Next, we examined mRNA levels of adrenergic receptors in
273 bone marrow cells differentiated to osteoclasts in our hands (Figure 7B). Consistent with the
274 RAW264.7 cell data, *Adrb2* was more highly expressed (Ct values are lower) than *Adrb1* (Figure
275 7B).
276 βARs have some agonist-independent signaling, and β-blockers can act as inverse
277 agonists to reduce this signaling, so we treated primary bone marrow cells with propranolol
278 while undergoing osteoclast differentiation. We examined the influence of 0.1, 1.0 and 10 μM
279 propranolol at day 7, when osteoclast differentiation has plateaued. In a concentration-dependent
280 manner, propranolol significantly reduced the number of multinucleated TRAP-positive cells
281 (Figure 7C, D), as well as reduced the hydroxyapatite area resorbed (Figure 7E, F). To ensure

Figure 7

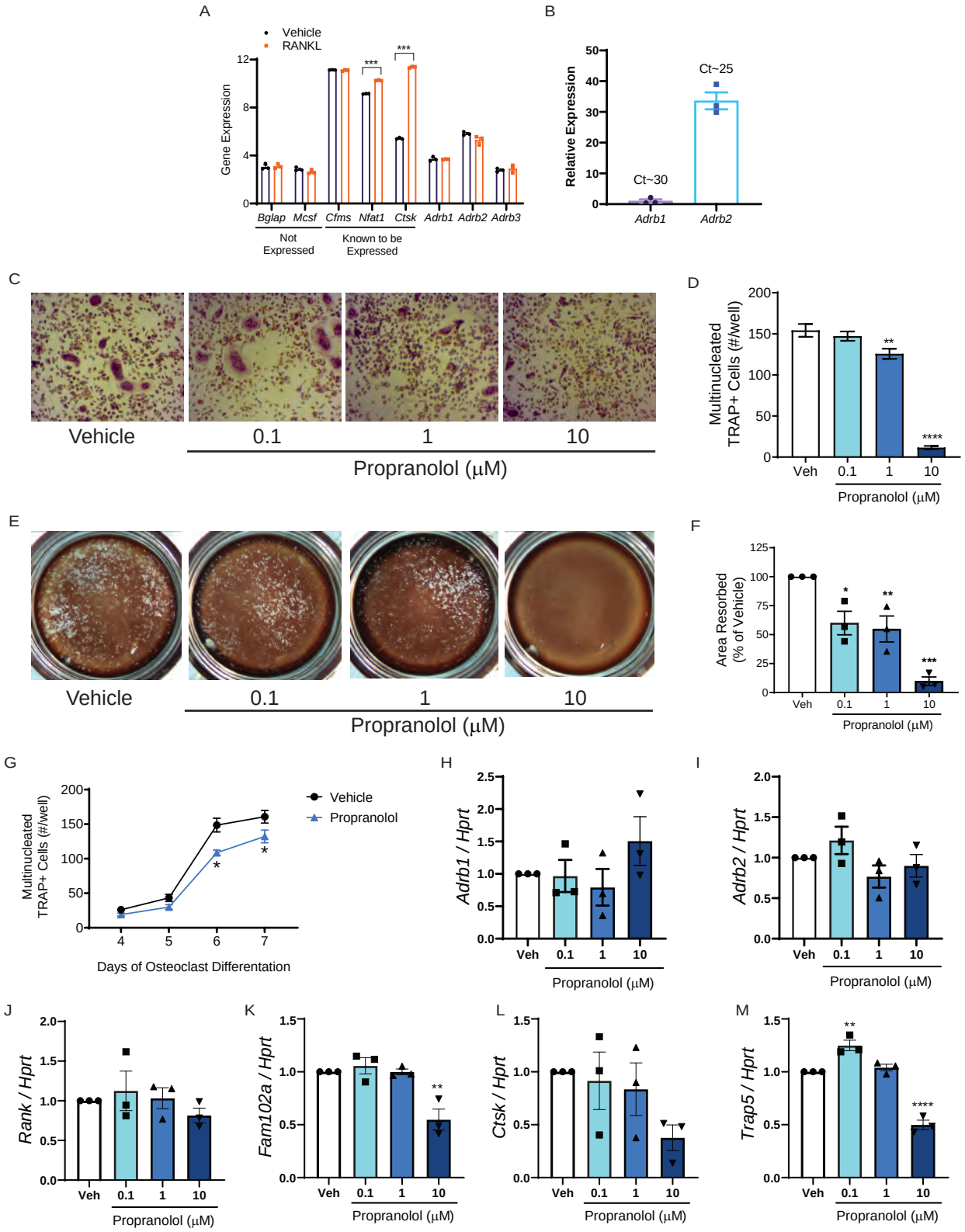
A
Vehicle
RANKL
Gene Expression
Bglap
Mcsf
Cfms
Nfat1
Ctsk
Adrb1
Adrb2
Adrb3
Not Expressed
Known to be Expressed
B
Relative Expression
Ct~25
Ct~30
Adrb1
Adrb2
C
Vehicle
0.1
1
10
Propranolol (μM)
D
Multinucleated TRAP+ Cells (#/well)
Veh
Propranolol (μM)
E
Vehicle
0.1
1
10
Propranolol (μM)
F
Area Resorbed (% of Vehicle)
Veh
Propranolol (μM)
G
Multinucleated TRAP+ Cells (#/well)
Vehicle
Propranolol
Days of Osteoclast Differentation
H
Adrb1 / Hprt
Veh
Propranolol (μM)
I
Adrb2 / Hprt
Veh
Propranolol (μM)
J
Rank / Hprt
Veh
Propranolol (μM)
K
Fam102a / Hprt
Veh
Propranolol (μM)
L
Ctsk / Hprt
Veh
Propranolol (μM)
M
Trap5 / Hprt
Veh
Propranolol (μM)

Figure 7. Osteoclast differentiation is impaired with propranolol treatment *in vitro*. (A) Publicly available microarray data from GEO, including *Adrb1*, *2* and *3*, as measured in RAW264.7 cells after 48-hour treatment with vehicle or RANKL. n=3/group. ***p<0.001 by Student's t-test. (B) Expression levels of *Adrb1* and *Adrb2* in primary bone marrow-derived osteoclasts. n=3. (C) Representative images of TRAP-stained osteoclasts that were differentiated in the presence of vehicle or 0.1, 1, or 10 μM propranolol. (D) One representative of four independent experiments where TRAP positive osteoclasts were counted in 96-well plates. (E) Representative OsteoAssay Surface plates stained for phosphate with a Von Kossa stain. White areas indicate surface that was resorbed by osteoclasts. (F) Quantification of three independent experiments, where the vehicle control for each was set to 100%. (D and F) *p<0.05, **p<0.01, ****p<0.0001 by Tukey's post hoc test after a significant one-way ANOVA. (G) Time course of primary bone marrow-derived osteoclast differentiation in the presence of vehicle or 1 μM propranolol. N=8 replicates per time point. *p<0.05 by Holm-Sidak post hoc test after a significant two-way ANOVA. (H-M) Gene expression normalized to housekeeping gene *Hprt* in primary osteoclasts treated with vehicle or indicated concentrations of propranolol. n=3 independent experiments with the vehicle control from each experiment set to 1. (H-M) *p<0.05, **p<0.01, ****p<0.0001 by Tukey's *post hoc* test after a significant one-way ANOVA. Bars represent mean +/- standard error.

282 that we were targeting an appropriate time point, we tested how 1.0 μM propranolol influenced
283 differentiation over time. Between days 5 and 6, there was a large increase in the number of
284 multinucleated, TRAP-positive osteoclasts, and this was attenuated with 1 μM propranolol
285 (Figure 7G). The difference between vehicle and propranolol treated number of osteoclasts
286 remained significant at day 7.

287 Expression of *Adrb1* and *Adrb2* were unchanged with increasing concentrations of
288 propranolol (Figure 7H, I). *Rank, Rela, Fos* and *Nfatc1,* genes involved with osteoclast
289 differentiation at earlier stages, were not affected by treatment with propranolol (Figure 7J and
290 not shown). However, consistent with the staining and resorption assays, propranolol dose-
291 dependently reduced gene expression of several key mid- to late-stage osteoclastogenic genes
292 and markers, including, *Fam102a, Ctsk*, and *Trap5* (Figure 7K-M), although *Ctsk* was too
293 variable to be called significant. Taken together, these findings suggest that propranolol directly
294 suppresses later stage osteoclast differentiation and function via β2AR.
295

296 **Discussion**

297 Here we show that propranolol and intermittent PTH co-treatment causes an improvement in
298 bone microarchitecture that exceeds that seen in intermittent PTH treatment alone, which is
299 consistent with previous co-treatment studies (Pierroz et al., 2006). We add to this, however, the
300 novel findings that propranolol enhances tissue mineral density, which may be through
301 promoting Ca^{2+} signaling pathway in osteoblasts. We are also the first to show that propranolol
302 prevents PTH-induced resorption and that this may be through direct inhibition of osteoclast
303 differentiation. In the absence of β-blockers, intermittent PTH treatment promotes both bone
304 formation *and* resorption, which could be of concern to individuals with severely lowered bone
305 density and/or high levels of resorption. Intracortical remodeling, which may lead to fracture, has
306 been associated with serum PTH levels in humans, as well as with daily intermittent PTH
307 treatment in rabbits (Osima et al., 2018; Zebaze et al., 2017). Nonetheless, PTH is very effective
308 at building new bone, so bone loss that occurs from heightened resorption needs to be weighed
309 against its anabolic activity. Our findings suggest that combining PTH with propranolol or other
310 β-blockers may be an attractive option to prevent unwanted bone loss in patients with very low
311 BMD.

312 The mechanism of propranolol action on bone to prevent resorption is likely in part
313 through direct effects of propranolol on osteoclasts. Neither PTH-induced serum RANKL nor
314 *Rankl* gene expression was suppressed by propranolol, despite clear improvement in trabecular
315 microarchitecture of the distal femur and the suppressed markers of resorption. The majority of
316 publications point toward osteoblast expression of RANKL as being the major mediator in the
317 effects of the sympathetic nervous system on osteoclasts (Elefteriou et al., 2005; Kajimura et al.,
318 2011). However, our findings suggest that this is not the same mechanism through which

319 propranolol blocks resorption. In studies examining the osteoblast-mediated mechanism of SNS-
320 induced bone loss, some experiments suggested no effect of *Adrb2* in osteoclasts. For example,
321 Elefteriou et al. elegantly showed that the non-specific βAR agonist isoproterenol only induces
322 osteoclast differentiation in osteoblast and bone marrow macrophage (BMM) co-cultures when
323 wildtype but not *Adrb2*$^{-/-}$ osteoblasts are present (Elefteriou et al., 2005). Similarly, the effect of
324 isoproterenol to induce osteoclast differentiation is not dependent upon the genotype of the
325 BMMs (Elefteriou et al., 2005). These data, in combination with findings from models with
326 osteoblast-specific deletions of *Adrb2*, have led to the generally accepted tenet that osteoblasts
327 are the sole mediators of the SNS effect on bone, including the mediators of osteoclast
328 recruitment (Kajimura et al., 2011).

329 There is a relative scarcity of literature examining the effects of β-adrenergic signaling
330 directly in osteoclasts. Rodrigues, et al. showed that propranolol prevented osteoclastogenesis of
331 RAW 264.7 cells through suppression of NFATc1 protein expression, as well as later markers of
332 differentiation: *Acp5, Ctsk,* and *Mmp9* (Rodrigues et al., 2012). This suggests a role for βAR
333 signaling in controlling NFATc1, which is under the control of calcium-calmodulin and
334 calcineurin signaling. Kondo, et al. demonstrated that isoproterenol enhanced osteoclastogenesis
335 in bone marrow macrophages and RAW 264.7 cells by increasing reactive oxygen species
336 (Kondo et al., 2013). Our findings are more aligned with these reports because we show
337 expression of *Adrb2* in primary bone marrow-derived osteoclasts, as well as a direct effect of
338 propranolol to suppress osteoclast differentiation. Although this is consistent with the other *in*
339 *vitro* reports, this mechanism remains to be established *in vivo*.

340 Despite the paucity of literature relating to the effects of the SNS in osteoclasts directly,
341 there is extensive evidence that *Adrb2* is expressed in other cells of the myeloid lineage and that

342 the SNS plays a role in their function (De Angelis et al., 2019). Indeed, the SNS is important for
343 the innate immune response required for tissue repair but can be pathologically activated during
344 certain conditions, such as in heart failure. β-blockers are a common therapeutic for heart failure
345 and they work in part by reducing inflammatory cytokine levels (De Angelis et al., 2019).
346 Systemic suppression of inflammation may also be an interesting, yet unexplored, avenue to
347 investigate the mechanism of efficacy of β-blockers in improving BMD, especially with regards
348 to resorption.

349 In contrast to our findings, global knockout of β2AR prevents any anabolic action of
350 PTH by preventing the PTH-induced increase in mineral apposition and osteoclast number
351 (Hanyu et al., 2012). Although these findings are paradoxical in some sense, they suggest that a
352 basal level of β2-adrenergic signaling in bone may be required for PTH action. It is also clear
353 that pharmaceutical inhibition of β2AR with propranolol is mechanistically distinct from the
354 disruption of signaling through genetic deletion. Propranolol can act as an inverse agonist,
355 meaning it has effects inhibitory toward cAMP signaling even when no agonist is present,
356 reducing spontaneous β2AR receptor activity (Baker, 2003). Furthermore, propranolol also binds
357 to the lesser expressed β1AR and is known to have non-specific effects, including acting as a
358 weak antagonist to some serotonin receptors, which could, in turn, impact bone remodeling
359 (Sozzani et al., 1992; Tinajero et al., 1993).

360 Moriya et al. showed that *Adrb2* knockdown enhances PTH-induced phosphorylation of
361 CREB, suggesting a suppressive function of β2AR on PTH action (Moriya et al., 2015). This is
362 consistent with our findings that PTH effects in osteoblasts are enhanced with pharmacological
363 β2AR inhibition. Some intracellular scaffolding proteins, such as members of the Na^+/H^+
364 exchange regulatory cofactor (NHERF) family, selectively promote coupling of the PTH1R to

365 the $G\alpha_q$-PLC-β signaling pathway(Cheloha et al., 2015). NHERF also couples β2AR to the
366 cytoskeleton, and agonist binding causes uncoupling from the cytoskeleton (Wheeler et al.,
367 2007). It is unknown, however, whether propranolol might uncouple β2AR from NHERF, G
368 proteins and/or the other signaling components, which could lead to the enhanced PTH-induced
369 Ca^{2+} flux (Figure 1B, C). Nonetheless, we observed enhanced *Igf1* expression after co-treatment
370 in osteoblasts, which has previously been shown work in an autocrine manner to stimulate
371 aerobic glycolysis in osteoblasts in response to PTH-treatment at 6 hours (Esen et al., 2015). In
372 our hands, elevation of *Igf1* after 1 hour of propranolol treatment suggests an acceleration of this
373 timetable, which may lead to the improved PTH effect on bone formation and tissue mineral
374 density that we observed *in vivo.*

375 TMD in the primary spongiosa was significantly higher with PTH and propranolol co-
376 treatment compared to PTH alone (Figure 3M). A similar trend was seen with cortical TMD
377 (Figure 4F) as well as total areal BMD assessed by DXA (Table I). Serum P1NP also indicated
378 global increases in bone formation with the combined treatment (Figure 5A), but this was not
379 observed in dynamic histomorphometric measurements of mineral apposition or bone formation
380 in the trabecular bone of the L5 vertebra (Figure 5C). However, gene expression in cortical bone
381 of the tibia suggested more mature osteoblasts/osteocytes (Figure 5G, H), indicating that
382 propranolol may have site-specific effects. Further studies investigating the mineral properties of
383 bone exposed to both PTH and propranolol would be necessary to determine if this combination
384 of treatments may improve strength in patients and animal models.

385 Clinical literature suggests that β-blockers prevent bone loss and reduce fracture risk in
386 humans. Yang et al. reported that β-blocker use was associated with a 17% decrease in risk of
387 fractures (Yang et al., 2012). Toulis et al. analyzed 16 studies involving over 1.5 million subjects

388 and found that the risk of fracture was significantly reduced (by 15%) in subjects receiving β-
389 blockers as compared to control subjects, independent of sex, fracture site, or dose (Toulis et al.,
390 2014). In contrast to what is the apparent mechanism in rodent models, β1-selective blockers
391 were found to be more effective at reducing fractures than non-selective β-blockers (i.e.
392 propranolol). More recently, when evaluating adrenergic receptor mRNA expression in human
393 bone biopsies, Khosla et al. found that ADRB1 and ADRB2, but not ADRB3, were expressed in
394 human bone (Khosla et al., 2018). Additionally, patients treated with β1-selective blockers had
395 better bone microarchitecture by quantitative computed tomography (qCT) than non-users, had
396 reduced CTx levels compared to placebo-treated patients, and had increased BMD at the
397 ultradistal radius, but these results were not seen in propranolol (non-selective β-blockers)
398 treated patients. Overall, this data suggests that β1-selective blockers are more protective against
399 decreased BMD and increased risk of fracture than non-selective β-blockers. Whether the
400 perceived difference between rodents and humans is due to β1AR being understudied in rodent
401 models or due to an actual species-specific difference in the relative importance of β1AR vs
402 β2AR in bone remains unclear.

403 Our findings reinforce the work of others suggesting that β-blockers, which are routinely
404 used clinically, may be an effective treatment or co-treatment for osteoporosis. Importantly, here
405 we showed that propranolol prevented resorption without modulating PTH-induced RANKL,
406 suggesting that the current understanding of the mechanism of β-blocker and sympathetic
407 nervous system action on bone is incomplete. Investigating the mechanisms of these effects,
408 whether through modulating osteoblast function or osteoclasts directly, will be necessary for the
409 accurate interpretation of clinical and preclinical studies examining how the sympathetic nervous
410 system modulates bone homeostasis and contributes to bone pathologies.

411 **Methods**

412 *Osteoblast assays*

413 MC3T3-E1 (clone 4) cells were purchased from ATCC and maintained at a low passage number
414 in α-MEM containing 1% penicillin streptomycin (P/S) and 10% fetal bovine serum (FBS). For
415 calcium assays, cells were plated overnight in 96-well black wall plates at a density of $5x10^4$
416 cells/well. Cells were then differentiated for 7 days with ascorbic acid and β-glycerophosphate as
417 previously described (Motyl et al., 2017). PTH (H-1660, Bachem) was aliquoted and stored in
418 glass vials at -70°C as a 10^{-4} M stock in 4 mM HCl supplemented with 0.1% bovine serum
419 albumin. PTH was thawed and diluted immediately prior to use. Propranolol hydrochloride
420 (P0884, Sigma-Aldrich) was dissolved in 1x HBSS buffer containing 20 mM HEPES for each
421 experiment. Calcium assays were performed with the FLIPR Calcium 6 Assay Kit (Molecular
422 Devices) according to the manufacturer's protocol. In brief, on day 7 of differentiation, cells
423 were incubated with calcium dye for two hours at 37°C and 5% CO_2. Then, fluorescence was
424 measured on a FlexStation 3 Multi-Mode Microplate Reader using SoftMax Pro 7 software
425 (Molecular Devices) in kinetic mode in response to additions of a range of concentrations of
426 PTH. Change in relative fluorescence units (maximum – minimum) is indicative of intracellular
427 calcium (iCa^{2+}) levels. Concentration-dependent change in max-min value was plotted on a
428 logarithmic scale and fit with a 4-parameter logistic curve to calculate the EC_{50}. In some
429 experiments, calcium dye incubation was concurrent with pretreatment with propranolol.
430 Additional 24-well plates were treated simultaneously with PTH and propranolol for 1 hour,
431 without the Calcium 6 reagents, and were saved for mRNA analyses.

432

433 *Mice and drug treatment*

434 Sixteen-week-old C57BL/6J (Jackson Laboratories, Bar Harbor, ME) female, intact mice
435 underwent baseline body weight measurements and were randomly assigned to one of four
436 treatment groups. Female mice were chosen because of their higher propensity to have an
437 anabolic response to intermittent PTH. Mice were treated with either vehicle, PTH, propranolol
438 or both PTH and propranolol. PTH aliquots were generated as above and thawed and diluted in
439 0.9% saline immediately prior to injection. Vehicle and PTH (80 μg/kg) were administered by
440 subcutaneous injection five days per week for four weeks. Propranolol hydrochloride oral
441 solution (West-Ward Pharmaceuticals) was dissolved in drinking water at a concentration of 0.5
442 mg/mL and was delivered daily for four weeks to animals in the propranolol and PTH +
443 propranolol groups as described (Motyl et al., 2015). At 20 weeks-of-age, mice were sacrificed
444 one hour after treatment and tissues were either fixed in 10% buffered formalin or snap-frozen in
445 liquid nitrogen and stored at -70°C. A similar study was conducted with just 5 days of treatment
446 to obtain additional samples for some mRNA and serum analyses and are identified in the figure
447 legends.
448
449 *Dual-energy X-ray absorptiometry (DXA)*
450 Mice underwent DXA measurements at baseline and at 20 weeks of age for fat-free mass, fat
451 mass, bone mineral density, and bone mineral content using the PIXImus dual-energy X-ray
452 densitometer (GE-Lunar, Madison, WI). The instrument was calibrated daily with a mouse
453 phantom provided by the manufacturer. Mice were anesthetized with isoflurane and placed
454 ventral side down with each limb and tail positioned away from the body. Full body scans were
455 obtained, and X-ray energy absorptiometry data were gathered and processed with manufacturer-

456 supplied software (Lunar PIXImus 2, version 2.1). The head was specifically excluded from all
457 analyses due to concentrated mineral in skull and teeth.
458
459 *Micro-computed tomography* (μCT)
460 A high-resolution desktop micro-tomographic imaging system (μCT40, Scanco Medical AG,
461 Bruttisellen, Switzerland) was used to assess the microarchitecture of the fifth lumbar (L5)
462 vertebral body and the femur in accordance with published guidelines (Bouxsein and Boyd,
463 2010). All analyses were performed using the Scanco Evaluation software.
464 In the L5 vertebra, scans were acquired using a resolution of 10 μm^3, 70 kVp peak x-ray tube
465 potential, 114 mA x-ray tube current, 200 ms integration time, and were subjected to Gaussian
466 filtration and segmentation. The endocortical region of the vertebral body was manually selected
467 beginning 100 μm inferior to the cranial growth plate and extending to 100 μm superior to the
468 caudal growth plate. Trabecular bone was segmented from soft-tissue using a threshold of 460
469 $mgHA/cm^3$. Measurements included trabecular bone volume fraction (Tb.BV/TV, %), trabecular
470 thickness (Tb.Th, mm), trabecular number (Tb.N, mm^{-1}), trabecular separation (Tb.Sp, mm),
471 connectivity density (Conn.D, mm^{-3}), and trabecular bone mineral density (Tb.BMD,
472 $mgHA/cm^3$).
473 To address microarchitecture in the primary and secondary spongiosa of the distal femur and
474 the cortical bone of the femur midshaft, scans were acquired with the same parameters used for
475 the L5 vertebrae. The primary spongiosa region of interest started at the peak of the distal growth
476 plate and extended proximally for 500 μm (50 transverse slices) and included the whole cross-
477 section of the bone. The secondary spongiosa region of interest started immediately superior to
478 the primary spongiosa region and extended 1500 μm (150 transverse slices) proximally and

479 included the endocortical region of the bone. In both regions, bone was segmented from soft-
480 tissue using a mineral density threshold of 460 mgHA/cm^3. Trabecular bone in the endocortical
481 area of the secondary spongiosa region was analyzed for bone volume fraction (Tb.BV/TV, %),
482 trabecular thickness (Tb.Th, mm), trabecular number (Tb.N, mm^{-1}), trabecular separation (Tb.Sp,
483 mm), connectivity density (Conn.D, mm^{-3}), and trabecular bone mineral density (Tb.BMD,
484 mgHA/cm^3). The bone in the primary spongiosa was analyzed for bone volume, total volume,
485 and bone mineral density.

486 Cortical bone architecture was analyzed in a 500 µm long region at the femoral mid-
487 diaphysis (55% of the total femur length inferior to the top of the femoral head). Cortical bone
488 was segmented from soft tissue using a threshold of 700 mgHA/cm^3. Measurements included
489 cortical bone area (Ct.Ar, mm^2), total cortical cross-sectional area (Tt.Ar, mm^2), cortical bone
490 area fraction (Ct.Ar/Tt.Ar, %), cortical thickness (Ct.Th, mm) and cortical porosity (%).

491

492 *Histology and Histomorphometry*

493 Tibiae were fixed in 10% neutral-buffered formalin and transferred to 70% ethanol after 24
494 hours. Samples were decalcified, paraffin-embedded, sectioned, and stained with hematoxylin
495 and eosin. Adipocyte size and number in the marrow in the region of the secondary spongiosa
496 were analyzed with BIOQUANT OSTEO software (BIOQUANT Image Analysis Corporation,
497 Nashville, TN). Total adipocyte area was divided by total area (marrow plus trabecular bone) in
498 the secondary spongiosa and multiplied by 100 to calculate adipocyte volume / total volume
499 (AV/TV). Adipocyte number was normalized to the total area measured.

500 Vertebrae were fixed in 10% neutral-buffered formalin and transferred to 70% ethanol
501 after 24 hours. The fixed lumbar vertebrae (L2-L5) were dehydrated with acetone and embedded

502 in methylmethacrylate. Undecalcified 4-µm-thick sections were obtained by microtome and
503 stained with Von Kossa method for showing the mineralized bone. The consecutive second
504 section was left unstained for the analysis of fluorescence labeling and the third section was
505 stained with 2% Toluidine Blue (pH 3.7) for the analysis of osteoblasts, osteoid, and osteoclasts.
506 The bone histomorphometric analysis was performed in the lumbar vertebra under 200X
507 magnification in a 1.35 mm high x 1.3 mm wide region where was located 400 µm away from
508 the upper and lower growth plate using OsteoMeasure analyzing software (Osteometrics Inc.,
509 Decatur, GA), in accordance with published guidelines (Dempster et al., 2013). The structural
510 parameters (BV/TV, Tb.Th, Tb.N, and Tb.Sp) were obtained by taking an average from two
511 different analysis of consecutive sections. The structural, dynamic and cellular parameters were
512 calculated and expressed according to the standardized nomenclature (Dempster et al., 2013).
513
514 *Enzyme Immunoassays*
515 Serum concentrations of amino-terminal propeptide of type 1 procollagen (P1NP), cross-linked
516 C-telopeptide (CTx) and TNF-related activation-induced cytokine (RANKL) were measured
517 with the Rat/Mouse P1NP enzyme immunoassay (EIA), RatLaps EIA (both from
518 Immunodiagnostic Systems, Scottsdale, AZ), and the Quantikine ELISA Mouse
519 TRANCE/RANKL/TNSFSF11 Kit (R&D Systems, Minneapolis, MN). The intraassay variations
520 were 6.3%, 6.9% and 4.3%, and the interassay variations were 8.5%, 12% and 6.9% respectively.
521 All measurements were performed in duplicate.
522
523 *RNA isolation and real-time PCR (qPCR)*

524 Total RNA was isolated from whole tibia and cortical shell using the standard TRIZOL (Sigma,
525 St. Louis, MO) method. Total RNA from cells was isolated using an RNeasy Mini Kit (Qiagen).
526 cDNA was synthesized using the High Capacity cDNA Reverse Transcriptase Kit (Applied
527 Biosystems, Foster City, CA) according to the manufacturer's instructions. mRNA expression
528 analysis was performed using an iQ SYBR Green Supermix or Taqman Gene Expression Assays
529 with an iQ5 thermal cycler and detection system (Bio-Rad, Hercules, CA). Hypoxanthine
530 guanine phosphoribosyl transferase (*Hprt*) was used as an internal standard control
531 gene(Vengellur and LaPres, 2004). Primer sequences are listed in the supplemental information
532 (Table S1).
533
534 *Norepinephrine extraction and measurements*
535 A volume of 20 µL of serum was combined with 100 µL of HPLC grade acetonitrile and vortex
536 mixed for two minutes. Subsequent to centrifugation at 14000 rpm for five minutes, the
537 supernatant was transferred to a 96-well plate for liquid chromatograph tandem mass
538 spectrometry (LC/MS-MS) analysis. A calibration curve was formed in mouse plasma from
539 0.305-2500 nM by serial dilution and extracted via the same methodology. An Agilent 1200
540 system consisting of a binary pump, column compartment and autosampler was used for solvent
541 delivery and sample introduction. Chromatographic separation was performed on a Phenomenex
542 Hydro RP 2.0 x 150 mm 4 µm column via a gradient using 0.1% formic acid in water (A) and
543 0.1% formic acid in acetonitrile (B). Gradient elution was 98% A from 0-1 minute, ramping to
544 50% A from 1.1 to 3.0 minutes, holding at 50% until 5.5 minutes, with re-equilibration at initial
545 conditions from 5.6 to 7.5 minutes. The flow rate was 0.30 mL/min, and column temperature was
546 30°C. Detection of norepinephrine was obtained using an Agilent 6460 triple quadrupole mass

Supplemental Table

Table SI. qPCR primer information.

Target Gene	Source/Supplier	Sequence	Catalog Number	Reference
Adrb1	Qiagen (Germantown, MD)	Not provided	330001, PPM05035A	N/A
Adrb2	Qiagen (Germantown, MD)	Not provided	330001, PPM04265A	N/A
Col1a1	Primer Design (Southampton, UK)	Forward: 5'-TCG TGG CTT CTC TGG TCT C-3' Reverse: 5'-CCG TTG AGT CCG TCT TTG C-3'	N/A	N/A
Ctsk	IDT (Coralvile, IA)	Forward: 5'-GCA GAG GTG TGT ACT ATG-3' Reverse: 5'-GCA GGC GTT GTT CTT ATT-3'	N/A	N/A
Dmp1	IDT (Coralvile, IA)	Forward: 5'-TCG CTG AGG TTT TGA CCT TGT-3' Reverse: 5'-CTC ACT GTT CGT GGG TGG TG-3'	N/A	(Motyl et al., 2015)
Fabp4	IDT (Coralvile, IA)	Forward: 5′-GCG TGG AAT TCG ATG AAA TCA-3′ Reverse: 5′-CCC GCC ATC TAG GGT TAT GA-3′	N/A	(Li et al., 2003)
Fos	Qiagen (Germantown, MD)	Not provided	330001, PPM02940C	N/A
Hprt	IDT (Coralvile, IA)	Forward: 5′-AAG CCT AAG ATG AGC GCA AG-3' Reverse: 5′-TTA CTA GGC AGA TGG CCA CA-3′	N/A	(Vengellur and LaPres, 2004)
Igf1	Primer Design (Southampton, UK)	Forward: 5'-GAC CGA GGG GCT TTT ACT TC-3' Reverse: 5'TGC TTT TGT AGG CTT CAG TGG-3'	N/A	N/A
Opg	IDT (Coralvile, IA)	Forward: 5'GAAGAAGATCATCCAAGACATTGAC-3' Reverse: 5'-TCCATAAACTGAGTAGCTTCAGGAG-3'	N/A	(Irwin et al., 2013)
Osteocalcin (Bglap)	IDT (Coralvile, IA)	Forward: 5'-ACG GTA TCA CTA TTT AGG ACC TGT-3' Reverse: 5'-ACT TTA TTT TGG AGC TGC TGT GAC-3'	N/A	(Ontiveros and McCabe, 2003)
Pth1r	IDT (Coralvile, IA)	Forward: 5'-TTT CCC GGT GCC TTC TCT TTC-3' Reverse: 5'-CAG GCG CAA TGT GAC AAG C-3'	N/A	(Ide et al., 2018)
Rankl	Primer Design (Southampton, UK)	Forward: 5'-TTT GCA CAC CTC ACC ATC AAT-3' Reverse: 5'- CCC TTA GTT TTC CGT TGC TTA AC-3'	N/A	N/A
Runx2	IDT (Coralvile, IA)	Forward: 5'-GAC AGA AGC TTG ATG ACT CTA AAC C-3' Reverse: 5'-TCT GTA ATC TGA CTC TGT CCT TGT G-3'	N/A	(Ontiveros et al., 2004)
Sost	Qiagen (Germantown, MD)	Not provided	330001, PPM36047A	N/A
Trap5 (Acp5)	IDT (Coralvile, IA)	Forward: 5'-AAT GCC TCG ACC TGG GA-3' Reverse: 5'-CGT AGT CCT CCT TGG CTG CT-3'	N/A	(Wiren et al., 2004)

547 spectrometer, monitoring the transition 152.0 → 107.0 with a fragmentor of 94 V and a collision
548 energy of 18 V. The retention time of norepinephrine was 1.37 minutes.
549
550 *Microarray Analyses*
551 Publicly available microarray data from RAW264.7 cells treated for 48 hours with RANKL and
552 vehicle was accessed from GEO (Gene Expression Omnibus, accession number GSE74847)
553 (Takigawa et al., 2016). Gene expression values were obtained after log2-transformation and
554 normalization to the Robust Multiarray Average (RMA).
555
556 *Osteoclast culture*
557 Primary osteoclasts were isolated from bone marrow from 6-8 week old female mice, as
558 previously described(Motyl et al., 2012). Briefly, bone marrow was plated and cultured with 30
559 ng/mL M-CSF and 50 ng/mL RANKL containing propranolol or vehicle for 6-7 days.
560 Osteoclasts were fixed in glutaraldehyde and stained for TRAP (387A-1KT, Sigma-Aldrich),
561 then TRAP-positive osteoclasts with 3 or more nuclei were counted. Corning OsteoAssay
562 Surfaces were stained for Von Kossa and resorbed area was quantified with ImageJ as previously
563 described(DeMambro et al., 2012). Additional osteoclasts cultured on plastic were saved for
564 mRNA analyses at day 7.
565
566 *Sample size estimation and statistics*
567 Sample size for mouse experiments was estimated based on previous experiments in our
568 laboratory using trabecular BV/TV as a primary outcome. Secondary outcomes of interest
569 included serum and histomorphometric indices of bone remodeling. All statistics were performed

570 with Prism 7 statistical software (GraphPad Software, Inc., La Jolla, CA). Results were analyzed
571 for statistically significant differences using one-way or two-way ANOVA followed by Tukey's
572 or Holm-Sidak multiple comparison *post hoc* tests, where appropriate. Statistical significance
573 was set at $p < 0.05$. All data are expressed as the mean ± standard error of the mean (SEM).
574 Outliers were handled as follows: first, any scientific/biological reason for the outlier was
575 investigated (i.e. sick mouse, degraded RNA, bad histology section); second, if no explanation
576 for the outlier was found we performed an outlier test to determine if the datum was > 3 standard
577 deviations (SD) from the mean of the other samples in that group. If the datum was > 3 SD from
578 the mean, it was excluded from further analysis. Outlier handling did not significantly change the
579 interpretation of the results.
580
581 *Study Approval*
582 The Institutional Animal Care and Use Committee of the Maine Medical Center Research
583 Institute approved all mouse protocols.

576 **Author Contributions**

577 AT was responsible for experimental design, data acquisition, data analysis, interpretation, and
578 drafting of the manuscript. ACB was responsible for experimental design, data acquisition, data
579 analysis, interpretation, drafting and critical review of the manuscript. DJB was responsible for
580 data acquisition, data analysis, interpretation, drafting of and critical revision of the manuscript.
581 HH was responsible for data acquisition, data analysis, interpretation and drafting of the
582 manuscript. KTN was responsible for data analysis, drafting and critical review of the
583 manuscript. KN was responsible for data acquisition, data analysis, interpretation, drafting of and
584 critical revision of the manuscript. DB was responsible for data acquisition, interpretation,
585 drafting and critical revision of the manuscript. KLH was responsible for experimental design,
586 data interpretation, drafting and critical revision of the manuscript. RB was responsible for data
587 interpretation and critical revision of the manuscript. MLB was responsible for data
588 interpretation and critical revision of the manuscript. ARG was responsible for experimental
589 design, data interpretation and critical revision of the manuscript. KJM was responsible for
590 experimental design, data acquisition, data analysis, interpretation, drafting and critical revision
591 of the manuscript. All authors had final approval of the manuscript.

592 **Acknowledgements**

593 The authors thank Adriana Lelis Carvalho and Audrie L. Langlais for critical evaluation of the
594 work. This work was supported by the National Institute of Arthritis And Musculoskeletal And
595 Skin Diseases (NIAMS) and the National Institute of General Medical Sciences (NIGMS) of the
596 National Institutes of Health (NIH) under award numbers K01AR067858 and P20GM121301 to
597 KJM. This work utilized services of the Maine Medical Center Research Institute (MMCRI)
598 Molecular Phenotyping Core, which is supported by NIH/NIGMS P30GM106391, the
599 Physiology Core, which is supported by NIH/NIGMS P30GM106391 and P20GM121301, the
600 Histopathology and Histomorphometry Core, which is supported by NIH/NIGMS
601 P30GM106391, P20GM121301, and P30103392, and the Mouse Transgenic and In Vivo
602 Imaging Core which is supported by NIH/NIGMS P30GM103392. All cores also received
603 support from the Norther New England Clinical and Translational Research Network
604 NIH/NIGMS U54GM115516. The content is solely the responsibility of the authors and does not
605 necessarily represent the official views of the National Institutes of Health.

606 **Figure Legends**

607 Figure 1. β-blocker propranolol potentiated osteoblast intracellular Ca^{2+} and *Igf1* expression.
608 MC3T3-E1 cells were differentiated to day 7 in osteogenic media. (A) Fluorescence ratio
609 indicative of intracellular Ca^{2+} concentrations was expressed as a percentage of the maximum
610 level. (B) Representative traces of 100 nM PTH-induced fluorescence over time with
611 pretreatment of vehicle, or 0.1, 1 or 10 μM propranolol. (C) Quantification of the maximum-
612 minimum PTH-induced Ca^{2+} fluorescence after pretreatment with vehicle or propranolol. One
613 representative of three experiments (each performed in triplicate) is shown. *p<0.05 compared to
614 vehicle-treated (black), ^p<0.05 compared to 100 nM PTH-treated (pink) by Tukey's *post-hoc*
615 test after significant one-way ANOVA. (D-K) Gene expression of *Runx2, Ocn, Fos, Igf1, Adrb1,*
616 *Adrb2, Pth1r* and *Igf1r* in MC3T3-E1 cells at day 7 after 1 hour treatment with vehicle (white),
617 100 nM PTH (pink), 1 μM propranolol (blue) or 100 nM PTH + 1 μM propranolol (purple).
618 Genes are normalized to non-modulated housekeeping gene, *Hprt*. Each data point represents the
619 mean from an independent experiment, performed in triplicate. Expression levels in vehicle-
620 treated cells from each experiment were set to 1. Approximate Ct values of vehicle-treated
621 groups are shown above each graph. Bars represent mean of the three independent experiments ±
622 SEM. *p<0.05, **p<0.01 by Holm-Sidak *post hoc* test after a significant two-way ANOVA.
623

624 Figure 2. Propranolol improved the positive effects of PTH on trabecular bone in the L5
625 vertebrae. Mice were treated with vehicle (white), 80 μg/kg PTH (light blue), 0.5 mg/ml
626 propranolol (gray), or PTH and propranolol (dark blue) for 4 weeks, from 16-20 weeks of age.
627 (A) Representative μCT images from L5 vertebrae. (B-G) Trabecular bone volume fraction (Tb.
628 BV/TV), bone mineral density (BMD), number (Tb.N), thickness (Tb.Th), separation (Tb.Sp),

629 and bone surface/bone volume (BS/BV). Bars represent mean ± standard error. *p<0.05,
630 **p<0.01 by Holm-Sidak *post hoc* test after a significant two-way ANOVA.
631
632 Figure 3. Trabecular bone in the femur secondary spongiosa is enhanced by combination PTH
633 and propranolol treatment. Mice were treated with vehicle (white), 80 µg/kg PTH (light blue),
634 0.5 mg/ml propranolol (gray), or PTH and propranolol (dark blue) for 4 weeks, from 16-20
635 weeks of age. (A) Representative 2D (top) and 3D (bottom) images of trabecular micro
636 architecture in the primary and secondary spongiosa of the distal femur. (B-I) Trabecular
637 microarchitectural parameters from the secondary spongiosa. (J-K) Volumetric and densitometric
638 measurements from the primary spongiosa. Bars represent mean ± standard error. *p<0.05,
639 **p<0.01, ***p<0.001, ****p<0.0001 by Holm-Sidak *post hoc* test after a significant two-way
640 ANOVA.
641
642 Figure 4. Propranolol improved cortical thickness and density in PTH-treated mice. Mice were
643 treated with vehicle (white), 80 µg/kg PTH (light blue), 0.5 mg/ml propranolol (gray), or PTH
644 and propranolol (dark blue) for 4 weeks, from 16-20 weeks of age. (A-H) Cortical bone
645 microarchitectural parameters, cortical area (Ct.Ar), marrow area (Ma.Ar), total area (Tt.Ar)
646 cortical area fraction (Ct.Ar/Tt.Ar), cortical thickness (Ct.Th), cortical tissue mineral density
647 (Ct.TMD), cortical porosity, and polar moment of inertia (pMOI) were analyzed at the midshaft
648 of the femur. Bars represent mean ± standard error. *p<0.05, **p<0.01 by Holm-Sidak *post hoc*
649 test after a significant two-way ANOVA.
650

651 Figure 5. Propranolol improved bone formation markers in PTH-treated mice. Mice were treated
652 with vehicle (white), 80 μg/kg PTH (light blue), 0.5 mg/ml propranolol (gray), or PTH and
653 propranolol (dark blue) for 4 weeks, from 16-20 weeks of age. (A) Serum P1NP was measured
654 by ELISA. (B-C) Static and dynamic histomorphometry representative images and quantification
655 of architectural, bone formation and osteoblast parameters measured in L5 vertebrae. (D-H)
656 Gene expression of markers of bone formation and osteoblast maturity were analyzed in the tibia
657 and normalized by the non-modulated housekeeping gene, *Hprt*. Bars represent mean ± standard
658 error. *$p<0.05$, **$p<0.01$ by Holm-Sidak *post hoc* test after a significant two-way ANOVA.
659
660 Figure 6. Propranolol prevented PTH-induced resorption but not RANKL induction. Mice were
661 treated for 4 weeks (A-F) with vehicle (white), 80 μg/kg PTH (light blue), 0.5 mg/ml propranolol
662 (gray), or PTH and propranolol (dark blue). (A-B) Gene expression of *Ctsk* and *Trap5* was
663 analyzed in the whole tibia and normalized by the non-modulated housekeeping gene, *Hprt*. (C)
664 Serum CTx was measured by ELISA. (D) Histomorphometric analyses of osteoclast and
665 resorption parameters were measured in L5 vertebrae. (E) Serum norepinephrine (NE) was
666 measured by LC/MS/MS. (F) Serum Rankl was measured by ELISA. (G-H) Mice were treated
667 with PTH and/or propranolol for 5 days and cortical shell was collected 1 hour after the last PTH
668 or vehicle dose. Gene expression levels of *Rankl* and *Opg* were normalized to *Hprt*. Bars
669 represent mean ± standard error. *$p<0.05$, **$p<0.01$, ***$p<0.001$ by Holm-Sidak *post hoc* test
670 after a significant two-way ANOVA.
671
672 Figure 7. Osteoclast differentiation is impaired with propranolol treatment *in vitro*. (A) Publicly
673 available microarray data from GEO, including *Adrb1, 2* and *3*, as measured in RAW264.7 cells

674 after 48-hour treatment with vehicle or RANKL. *n*=3/group. ***$p<0.001$ by Student's t-test. (B)
675 Expression levels of *Adrb1* and *Adrb2* in primary bone marrow-derived osteoclasts. *n*=3. (C)
676 Representative images of TRAP-stained osteoclasts that were differentiated in the presence of
677 vehicle or 0.1, 1, or 10 μM propranolol. (D) One representative of four independent experiments
678 where TRAP positive osteoclasts were counted in 96-well plates. (E) Representative OsteoAssay
679 Surface plates stained for phosphate with a Von Kossa stain. White areas indicate surface that
680 was resorbed by osteoclasts. (F) Quantification of three independent experiments, where the
681 vehicle control for each was set to 100%. (D and F) *$p<0.05$, **$p<0.01$, ****$p<0.0001$ by
682 Tukey's *post hoc* test after a significant one-way ANOVA. (G) Time course of primary bone
683 marrow-derived osteoclast differentiation in the presence of vehicle or 1 μM propranolol. N=8
684 replicates per time point. *$p<0.05$ by Holm-Sidak *post hoc* test after a significant two-way
685 ANOVA. (H-M) Gene expression normalized to housekeeping gene *Hprt* in primary osteoclasts
686 treated with vehicle or indicated concentrations of propranolol. *n*=3 independent experiments
687 with the vehicle control from each experiment set to 1. (H-M) *$p<0.05$, **$p<0.01$, ****$p<0.0001$
688 by Tukey's *post hoc* test after a significant one-way ANOVA. Bars represent mean ± standard
689 error.
690
691 Figure S1. Effects of PTH and propranolol on proximal tibia bone marrow adiposity. Mice were
692 treated for 4 weeks with vehicle (white), 80 μg/kg PTH (light blue), 0.5 mg/ml propranolol
693 (gray), or PTH and propranolol (dark blue). (A) Tibias were decalcified and stained with H & E.
694 Scale bar = 500 μm. (B-D) Adipocyte ghosts were measured using BIOQUANT OSTEO
695 software. (E) *Fabp4* gene expression was measured in whole tibia and normalized to non-
696 modulated housekeeping gene *Hprt.* Bars represent mean ± standard error. Indicated *p*-values

697 were determined by Holm-Sidak *post hoc* test after a significant interaction effect was found
698 using two-way ANOVA.
699
700 **References**

701 Baek K, Park HJ, Hwang HR, Baek JH. 2014. Propranolol attenuates calorie restriction- and high
702 calorie diet-induced bone marrow adiposity. *BMB Rep*.
703 doi:10.5483/BMBRep.2014.47.10.176
704 Baker JG. 2003. Agonist and Inverse Agonist Actions of -Blockers at the Human 2-
705 Adrenoceptor Provide Evidence for Agonist-Directed Signaling. *Mol Pharmacol*.
706 doi:10.1124/mol.64.6.1357
707 Bellido T, Ali AA, Gubrij I, Plotkin LI, Fu Q, O'Brien CA, Manolagas SC, Jilka RL. 2005.
708 Chronic elevation of parathyroid hormone in mice reduces expression of sclerostin by
709 osteocytes: A novel mechanism for hormonal control of osteoblastogenesis. *Endocrinology*.
710 doi:10.1210/en.2005-0239
711 Bouxsein M, Boyd S. 2010. Guidelines for assessment of bone microstructure in rodents using
712 micro–computed tomography. *J bone ...* **25**:1468–86. doi:10.1002/jbmr.141
713 Cheloha RW, Gellman SH, Vilardaga JP, Gardella TJ. 2015. PTH receptor-1 signalling -
714 Mechanistic insights and therapeutic prospects. *Nat Rev Endocrinol*.
715 doi:10.1038/nrendo.2015.139
716 De Angelis E, Pecoraro M, Rusciano MR, Ciccarelli M, Popolo A. 2019. Cross-talk between
717 neurohormonal pathways and the immune system in heart failure: A review of the literature.
718 *Int J Mol Sci*. doi:10.3390/ijms20071698
719 DeMambro VE, Maile L, Wai C, Kawai M, Cascella T, Rosen CJ, Clemmons D. 2012. Insulin-

720 like growth factor-binding protein-2 is required for osteoclast differentiation. *J Bone Min*
721 *Res* **27**:390–400. doi:10.1002/jbmr.545
722 Dempster DW, Compston JE, Drezner MK, Glorieux FH, Kanis JA, Malluche H, Meunier PJ,
723 Ott SM, Recker RR, Parfitt AM. 2013. Standardized Nomenclature, Symbols, and Units for
724 Bone Histomorphometry: A 2012 Update of the Report of the ASBMR Histomorphometry
725 Nomenclature Committee. *J Bone Min Res* **28**:2–17. doi:10.1002/jbmr.1805
726 Ducy P, Amling M, Takeda S, Priemel M, Schilling AF, Beil FT, Shen J, Vinson C, Rueger JM,
727 Karsenty G. 2000. Leptin inhibits bone formation through a hypothalamic relay: a central
728 control of bone mass. *Cell* **100**:197–207.
729 Elefteriou F, Ahn JD, Takeda S, Starbuck M, Yang X, Liu X, Kondo H, Richards WG, Bannon
730 TW, Noda M, Clement K, Vaisse C, Karsenty G. 2005. Leptin regulation of bone resorption
731 by the sympathetic nervous system and CART. *Nature* **434**:514–520.
732 doi:10.1038/nature03398
733 Esen E, Lee SY, Wice BM, Long F. 2015. PTH Promotes Bone Anabolism by Stimulating
734 Aerobic Glycolysis via IGF Signaling. *J Bone Miner Res*. doi:10.1002/jbmr.2556
735 Fan Y, Hanai JI, Le PT, Bi R, Maridas D, DeMambro V, Figueroa CA, Kir S, Zhou X,
736 Mannstadt M, Baron R, Bronson RT, Horowitz MC, Wu JY, Bilezikian JP, Dempster DW,
737 Rosen CJ, Lanske B. 2017. Parathyroid Hormone Directs Bone Marrow Mesenchymal Cell
738 Fate. *Cell Metab* **25**:661–672. doi:10.1016/j.cmet.2017.01.001
739 Gesty-Palmer D, Luttrell LM. 2011. "Biasing" the parathyroid hormone receptor: A novel
740 anabolic approach to increasing bone mass? *Br J Pharmacol*. doi:10.1111/j.1476-
741 5381.2011.01450.x
742 Hanyu R, Wehbi VL, Hayata T, Moriya S, Feinstein TN, Ezura Y, Nagao M, Saita Y, Hemmi H,

743 Notomi T, Nakamoto T, Schipani E, Takeda S, Kaneko K, Kurosawa H, Karsenty G,
744 Kronenberg HM, Vilardaga JP, Noda M. 2012. Anabolic action of parathyroid hormone
745 regulated by the beta2-adrenergic receptor. *Proc Natl Acad Sci U S A* **109**:7433–7438.
746 doi:10.1073/pnas.1109036109
747 Jean-Alphonse FG, Wehbi VL, Chen J, Noda M, Taboas JM, Xiao K, Vilardaga JP. 2017. β 2 -
748 adrenergic receptor control of endosomal PTH receptor signaling via Gβ 3. *Nat Chem Biol*.
749 doi:10.1038/nchembio.2267
750 Kajimura D, Hinoi E, Ferron M, Kode A, Riley KJ, Zhou B, Guo XE, Karsenty G. 2011. Genetic
751 determination of the cellular basis of the sympathetic regulation of bone mass accrual. *J Exp*
752 *Med*. doi:10.1084/jem.20102608
753 Khosla S, Monroe DG, Farr JN. 2018. Sympathetic b 1 -adrenergic signaling contributes to
754 regulation of human bone metabolism Graphical abstract Find the latest version : *J Clin*
755 *Invest*.
756 Kondo H, Takeuchi S, Togari A. 2013. beta-Adrenergic signaling stimulates osteoclastogenesis
757 via reactive oxygen species. *Am J Physiol Endocrinol Metab* **304**:E507-15.
758 doi:10.1152/ajpendo.00191.2012
759 Mach DB, Rogers SD, Sabino MC, Luger NM, Schwei MJ, Pomonis JD, Keyser CP, Clohisy
760 DR, Adams DJ, O'Leary P, Mantyh PW. 2002. Origins of skeletal pain: sensory and
761 sympathetic innervation of the mouse femur. *Neuroscience* **113**:155–166.
762 Moriya S, Hayata T, Notomi T, Aryal S, Nakamaoto T, Izu Y, Kawasaki M, Yamada T,
763 Shirakawa J, Kaneko K, Ezura Y, Noda M. 2015. PTH regulates β2-adrenergic receptor
764 expression in osteoblast-like MC3T3-E1 cells. *J Cell Biochem*. doi:10.1002/jcb.24953
765 Motyl KJ, Beauchemin M, Barlow D, Le PT, Nagano K, Treyball A, Contractor A, Baron R,

766 Rosen CJ, Houseknecht KL. 2017. A novel role for dopamine signaling in the pathogenesis
767 of bone loss from the atypical antipsychotic drug risperidone in female mice. *Bone*
768 **103**:168–176. doi:10.1016/j.bone.2017.07.008
769 Motyl KJ, Bishop KA, Demambro VE, Bornstein SA, Le P, Kawai M, Lotinun S, Horowitz MC,
770 Baron R, Bouxsein ML, Rosen CJ. 2013. Altered thermogenesis and impaired bone
771 remodeling in Misty mice. *J Bone Miner Res* **28**. doi:10.1002/jbmr.1943
772 Motyl KJ, DeMambro VE, Barlow D, Olshan D, Nagano K, Baron R, Rosen CJ, Houseknecht
773 KL. 2015. Propranolol attenuates risperidone-induced trabecular bone loss in female mice.
774 *Endocrinology* **156**. doi:10.1210/en.2015-1099
775 Motyl KJ, Dick-de-Paula I, Maloney AE, Lotinun S, Bornstein S, de Paula FJA, Baron R,
776 Houseknecht KL, Rosen CJ. 2012. Trabecular bone loss after administration of the second-
777 generation antipsychotic risperidone is independent of weight gain. *Bone* **50**.
778 doi:10.1016/j.bone.2011.08.005
779 Ortuno MJ, Robinson ST, Subramanyam P, Paone R, Huang YY, Guo XE, Colecraft HM, Mann
780 JJ, Ducy P. 2016. Serotonin-reuptake inhibitors act centrally to cause bone loss in mice by
781 counteracting a local anti-resorptive effect. *Nat Med* **22**:1170–1179. doi:10.1038/nm.4166
782 Osima M, Borgen TT, Lukic M, Grimnes G, Joakimsen RM, Eriksen EF, Bjørnerem. 2018.
783 Serum parathyroid hormone is associated with increased cortical porosity of the inner
784 transitional zone at the proximal femur in postmenopausal women: the Tromsø Study.
785 *Osteoporos Int*. doi:10.1007/s00198-017-4298-3
786 Pierroz DD, Bouxsein ML, Rizzoli R, Ferrari SL. 2006. Combined treatment with a beta-blocker
787 and intermittent PTH improves bone mass and microarchitecture in ovariectomized mice.
788 *Bone* **39**:260–267. doi:10.1016/j.bone.2006.01.145

789 Rodrigues WF, Madeira MFM, da Silva TA, Clemente-Napimoga JT, Miguel CB, Dias-da-Silva
790 VJ, Barbosa-Neto O, Lopes AH, Napimoga MH. 2012. Low dose of propranolol down-
791 modulates bone resorption by inhibiting inflammation and osteoclast differentiation. *Br J*
792 *Pharmacol* **165**:2140–2151. doi:10.1111/j.1476-5381.2011.01686.x
793 Sozzani S, Agwu DE, McCall CE, O'Flaherty JT, Schmitt JD, Kent JD, McPhail LC. 1992.
794 Propranolol, a phosphatidate phosphohydrolase inhibitor, also inhibits protein kinase C. *J*
795 *Biol Chem*.
796 Takeda S, Elefteriou F, Levasseur R, Liu X, Zhao L, Parker KL, Armstrong D, Ducy P, Karsenty
797 G. 2002. Leptin regulates bone formation via the sympathetic nervous system. *Cell*
798 **111**:305–317.
799 Takigawa S, Chen A, Wan Q, Na S, Sudo A, Yokota H, Hamamura K. 2016. Role of miR-222-
800 3p in c-Src-Mediated Regulation of Osteoclastogenesis. *Int J Mol Sci*.
801 doi:10.3390/ijms17020240
802 Tinajero JC, Fabbri A, Dufau ML. 1993. Serotonergic inhibition of rat leydig cell function by
803 propranolol. *Endocrinology*. doi:10.1210/endo.133.1.8391422
804 Toulis KA, Hemming K, Stergianos S, Nirantharakumar K, Bilezikian JP. 2014. β-adrenergic
805 receptor antagonists and fracture risk: A meta-analysis of selectivity, gender, and site-
806 specific effects. *Osteoporos Int*. doi:10.1007/s00198-013-2498-z
807 Vengellur A, LaPres JJ. 2004. The role of hypoxia inducible factor 1α in cobalt chloride induced
808 cell death in mouse embryonic fibroblasts. *Toxicol Sci*. doi:10.1093/toxsci/kfh278
809 Wheeler D, Sneddon WB, Wang B, Friedman PA, Romero G. 2007. NHERF-1 and the
810 cytoskeleton regulate the traffic and membrane dynamics of G protein-coupled receptors. *J*
811 *Biol Chem*. doi:10.1074/jbc.M701544200

812 Yadav VK, Oury F, Suda N, Liu ZW, Gao XB, Confavreux C, Klemenhagen KC, Tanaka KF,
813 Gingrich JA, Guo XE, Tecott LH, Mann JJ, Hen R, Horvath TL, Karsenty G. 2009. A
814 serotonin-dependent mechanism explains the leptin regulation of bone mass, appetite, and
815 energy expenditure. *Cell* **138**:976–989. doi:10.1016/j.cell.2009.06.051
816 Yang S, Nguyen ND, Eisman JA, Nguyen T V. 2012. Association between beta-blockers and
817 fracture risk: A Bayesian meta-analysis. *Bone*. doi:10.1016/j.bone.2012.07.013
818 Yirmiya R, Goshen I, Bajayo A, Kreisel T, Feldman S, Tam J, Trembovler V, Csernus V,
819 Shohami E, Bab I. 2006. Depression induces bone loss through stimulation of the
820 sympathetic nervous system. *Proc Natl Acad Sci U S A* **103**:16876–16881.
821 doi:10.1073/pnas.0604234103
822 Zayzafoon M, Fulzele K, McDonald JM. 2005. Calmodulin and calmodulin-dependent kinase IIα
823 regulate osteoblast differentiation by controlling c-fos expression. *J Biol Chem*.
824 doi:10.1074/jbc.M412680200
825 Zebaze R, Takao-Kawabata R, Peng Y, Zadeh AG, Hirano K, Yamane H, Takakura A, Isogai Y,
826 Ishizuya T, Seeman E. 2017. Increased cortical porosity is associated with daily, not
827 weekly, administration of equivalent doses of teriparatide. *Bone*.
828 doi:10.1016/j.bone.2017.03.042
829

Supplemental References

Ide N, Ye R, Courbebaisse M, Olauson H, Densmore MJ, Larsson TE, Hanai JI, Lanske B. 2018. In vivo evidence for an interplay of FGF23/Klotho/PTH axis on the phosphate handling in renal proximal tubules. *Am J Physiol - Ren Physiol*. doi:10.1152/ajprenal.00650.2017

Irwin R, Lee T, Young VB, Parameswaran N, McCabe LR. 2013. Colitis-induced bone loss is gender dependent and associated with increased inflammation. *Inflamm Bowel Dis* **19**:1586–1597. doi:10.1097/MIB.0b013e318289e17b

Li J, Takaishi K, Cook W, McCorkle SK, Unger RH. 2003. Insig-1 "brakes" lipogenesis in adipocytes and inhibits differentiation of preadipocytes. *Proc Natl Acad Sci U S A*. doi:10.1073/pnas.1133426100

Motyl KJ, DeMambro VE, Barlow D, Olshan D, Nagano K, Baron R, Rosen CJ, Houseknecht KL. 2015. Propranolol attenuates risperidone-induced trabecular bone loss in female mice. *Endocrinology* **156**. doi:10.1210/en.2015-1099

Ontiveros C, Irwin R, Wiseman RW, McCabe LR. 2004. Hypoxia suppresses runx2 independent of modeled microgravity. *J Cell Physiol* **200**:169–176. doi:10.1002/jcp.20054

Ontiveros C, McCabe LR. 2003. Simulated microgravity suppresses osteoblast phenotype, runx2 levels and AP-1 transactivation. *J Cell Biochem*. doi:10.1002/jcb.10410

Vengellur A, LaPres JJ. 2004. The role of hypoxia inducible factor 1α in cobalt chloride induced cell death in mouse embryonic fibroblasts. *Toxicol Sci*. doi:10.1093/toxsci/kfh278

Wiren KM, Zhang XW, Toombs AR, Kasparcova V, Gentile MA, Harada SI, Jepsen KJ. 2004. Targeted overexpression of androgen receptor in osteoblasts: Unexpected complex bone phenotype in growing animals. *Endocrinology*. doi:10.1210/en.2003-1016